



# Three-dimensional liquid chromatography with parallel second dimensions and quadruple parallel mass spectrometry for adult/infant formula analysis



William Craig Byrdwell<sup>a,\*</sup>, Hari K. Kotapati<sup>a</sup>, Robert Goldschmidt<sup>a</sup>, Pavel Jakubec<sup>b</sup>, Lucie Nováková<sup>b</sup>

<sup>a</sup> Methods and Application of Food Composition Lab, Agricultural Research Service, U.S. Dept. of Agriculture, 10300 Baltimore Ave., Beltsville, MD, 20705, USA

<sup>b</sup> Charles University, Faculty of Pharmacy, Dept. of Analytical Chemistry, Heyrovského 1203, 500 05 Hradec Králové, Czech Republic

## ARTICLE INFO

### Article history:

Received 21 September 2021

Revised 5 November 2021

Accepted 9 November 2021

Available online 22 November 2021

### Keywords:

3D-LC

2D-LC

Two-dimensional LC

APPI-MS

ESI-MS

Lipidomics

## ABSTRACT

Three dimensions of chromatographic separation, using split-flow two-dimensional liquid chromatography (SF-2D-LC) with two parallel second dimensions, LC × 2LC, combined with quadruple parallel mass spectrometry (LC3MS4) is demonstrated for analysis of NIST SRM 1849a adult/infant formula. The first dimension, <sup>1</sup>D, was a conventional non-aqueous reversed-phase (NARP) HPLC separation using two C18 columns in series, followed by detection using an ultraviolet (UV) detector, a fluorescence detector (FLD), with flow then split to a corona charged aerosol detector (CAD), and then dual parallel mass spectrometry (MS), conducted in atmospheric pressure photoionization (APPI) and electrospray ionization (ESI) modes. The first second dimension, <sup>2</sup>D(1), UHPLC was conducted on a 50.0 mm C30 column using a NARP-UHPLC parallel gradient for separation of short-chain triacylglycerols (TAGs) from long-chain TAGs, with detection by UV and ESI-MS. The second dimension, <sup>2</sup>D(2), UHPLC was conducted using a 100.0 mm C30 column with a NARP-UHPLC parallel gradient for improved separation of TAG isomers, with detection by UV, an evaporative light scattering detector, and high-resolution, accurate-mass (HRAM) ESI-MS. Transferred eluent dilution was used to refocus peaks and keep them sharp during elution in both <sup>2</sup>Ds. The separation space in the <sup>2</sup>D(2) was optimized using multi-cycle (aka, “constructive wraparound”) elution, which employed flow rate programming. In the <sup>1</sup>D, calibration lines for quantification of fat-soluble vitamins were constructed. A lipidomics approach to TAG identification and quantification by HRAM-ESI-MS was applied to the <sup>2</sup>D(2). These experiments can be represented: LC1MS2 × (LC1MS1 + LC1MS1) = LC3MS4, or three-dimensional liquid chromatography with quadruple parallel mass spectrometry.

Published by Elsevier B.V.

## 1. Introduction

Two-dimensional liquid chromatography, 2D-LC, has become increasingly popular as commercially available systems have become routinely available. Although it is more complex than conventional 1D-LC and requires two instruments, a switching valve, and specialized software to operate, the advantages of 2D-LC often far outweigh the disadvantages of additional complexity and expense. There are many separations that simply cannot be performed as effectively using 1D-LC. Peak capacities can be greatly increased using 2D-LC, and at the theoretical limit, the peak capacities are multiplicative [1,2]. Based on several available tutorials [3–6], some of the principles and nomenclature that most apply to the work de-

scribed here are as follows. Comprehensive 2D-LC, or LC × LC, describes a process in which [4]: 1) every part of the sample is subjected to two different separations (in other words, every peak separated in the first dimension, <sup>1</sup>D, has a corresponding peak in the second dimension, <sup>2</sup>D); 2) equal percentages (either 100% or lower) of all sample components pass through both columns and eventually reach the detector; and 3) the separation (resolution) obtained in the first dimension is essentially maintained. This is distinct from heart-cutting and selective comprehensive approaches, in which only a subset of peaks is separated in two dimensions. In most 2D-LC systems the flow path is closed, such that all of the flow from the <sup>1</sup>D goes to the second dimension, <sup>2</sup>D, according to criterion #2, above. Usually, detection is done at the outlet of the <sup>2</sup>D, and the <sup>1</sup>D is reconstructed from multiple chops, or modulations, across the <sup>1</sup>D peaks. An insufficient number of modulations across a peak is referred to as ‘undersampling’, and results in inaccurate reproduction of the first dimension.

\* Corresponding author.

E-mail address: [Craig.Byrdwell@usda.gov](mailto:Craig.Byrdwell@usda.gov) (W.C. Byrdwell).

These conditions impose some severe restrictions on the instruments and conditions used for 2D-LC. First, the  $^2D$  separations must be very fast to allow enough modulations across  $^1D$  peaks to avoid undersampling. This is often accomplished with very high to extremely high flow rates in the second dimension to yield fast runs, which limits separation flexibility in the  $^2D$ . Second, since all of the effluent from the  $^1D$  is directed to the  $^2D$ , solvent incompatibility issues are often encountered, especially when using very disparate stationary phases and solvent compositions to give highly 'orthogonal' separations (having very different polarities and retention mechanisms). Solvent incompatibility has often been addressed by using small-bore columns in the first dimension with low flow rates to minimize the amount of solvent transferred, which is diluted by very high flow rates in the  $^2D$ . More recently, active solvent modulation (ASM), has been implemented in these closed systems to help to mitigate solvent incompatibility issues [7]. While this does add to the complexity of plumbing and expense, it is now readily available as an addition to commercial 2D-LC systems. Another restriction imposed by the above conditions is the need for very fast-scanning detectors, especially mass spectrometers, to be able to get multiple scans across the very narrow  $^2D$  peaks that result from such fast  $^2D$  separations. Thus, the whole system must be optimized for fast separations and fast detection, which means that only newer and more expensive instrumentation is capable of such analyses. One last restriction is that commercial 2D-LC systems are designed for, and only allow one  $^2D$  coupled to a  $^1D$ , since again, all flow from the  $^1D$  normally goes onto the  $^2D$  column.

Gas chromatography (GC) is a more mature field than liquid chromatography, and numerous innovative experiments have been reported that combine different combinations of dual parallel second dimensions [8–12], referred to as  $GC \times 2GC$ . Other researchers used parallel multiplexed GC first dimensions that went to a single second dimension [13], referred to as  $2GC \times GC$ . A recent groundbreaking approach was described that used two parallel first dimensions and two parallel second dimensions [14], referred to as  $2GC \times 2GC$ . Most experiments employed the flame ionization detector (FID) [8–11,14], but MS was also used in  $GC \times 2GC$  for detection of one of the parallel second dimensions ( $GC \times (GC-FID + GC-MS)$ ) [12]. MS was also used in the experiments for  $2GC \times GC-MS$  [13]. By analogy, the experiments reported here may be referred to as  $LC \times 2LC$  to describe the liquid chromatography aspects of these experiments, though a more thorough description that includes the quadruple parallel mass spectrometers spread across three dimensions of separation is given below.

Ever since the Yates group introduced multi-dimensional protein identification technology (MudPIT) [15,16] using 2D-LC-MS, multi-dimensional approaches have been widely used for proteins, and there have been repeated demonstrations of using more than two dimensions of separation. Numerous three-dimensional LC separations have been reported, which have been mostly applied to bottom-up proteomics. These applications have been recently reviewed [17]. Many of the examples include offline components, such as fraction collection and re-injection [18], so are not germane to the current report of online parallel second dimensions. A recent example for the quantification of two alkaloids employed three dimensions of separation with fraction collection and re-injection between each separation [18]. A rather early example of an online 3D-LC analysis of yeast was reported by Wei et al. [19], in which three columns were joined together, and different wash cycles eluted analytes to a mass spectrometer. An example of online 3D-LC in which the first stage pre-fractionation was automated and transferred to a 2D-LC system was used for separation of a soybean extract [20]. A recent example of a "middle-up" approach to analysis of large fragments of proteins [21] used online 3D-LC with enzymatic digestion of proteins in the first col-

umn, followed by reduction in the second column, and then analysis by hydrophilic interaction LC (HILIC) in the third column with detection by HRAM-MS. A non-proteomics early example of heart-cutting 3D-LC, in which targeted windows of elution were transferred to a second dimension and targeted windows from that separation were transferred to a third separation was demonstrated by Simpkins et al. [22]. None of the examples of 3D-LC we have found have included the kind of online comprehensive 3D-LC with multiple parallel mass spectrometers reported here. However, we did find references [22–24] to eluent dilution that is similar to the transferred eluent dilution (TED) that we have employed here.

We became interested in 2D-LC due to the need to separate triacylglycerols (TAGs) containing *cis*- and *trans*-fatty acids (FA) [25,26]. We combined non-aqueous reversed-phase (NARP) HPLC with silver-ion UHPLC to separate TAGs first by equivalent carbon number ( $ECN = \text{carbon number (CN)} - 2 \times \# \text{ double bonds}$ ), then to further separate TAGs by degree and location of unsaturation. To accomplish those experiments, we implemented a unique approach to bypass problems inherent in conventional 2D-LC analyses reported in the past. Several aspects of our unique approach are described here, since they are retained and expanded upon in this work to allow an extended range of unconventional experiments to be performed.

The most important aspects that are critical to our approach are: 1) Analysis using dual parallel mass spectrometry [27–31], LC1MS2, plus several other detectors (ultraviolet (UV), corona charged aerosol detector (CAD), and fluorescence detector (FLD)) to directly detect the  $^1D$ , thereby eliminating the need for fast sampling of the  $^2D$  to reproduce the  $^1D$  and bypassing the problem of undersampling, as well as allowing conventional quantification by selected ion monitoring (SIM) and selected reaction monitoring (SRM) and detection by UV. This was combined with dual parallel mass spectrometry in the  $^2D$ , for  $LC1MS2 \times LC1MS2 = LC2MS4$  [25,26]. 2) Using split-flow comprehensive 2D-LC (SF-C2DLC) instead of a closed system, such that only a proportion of the  $^1D$  eluent was directed to the  $^2D$ . 3) Employing a wireless communication contact closure system (WCCCS) [32] to coordinate all instrument starts, auto-zeroes, and syringe pump refills.

In this report, we build on the various aspects from our earlier reports described above and expand them for the experiments reported here. The innovations developed for these experiments include: 1) Use of a second dimension,  $^2D(2)$ , to provide two parallel second dimensions of separation for three dimensions of separation overall, for  $LC \times 2LC$  or 3D-LC. 2) Development of a prototype  $^2D$  valve switching system [33] employing a timed contact closure circuit (TCCC) controlled by a relay in the WCCCS to automate valve changes with a constant modulation period. 3) Implementation of transferred eluent dilution (TED) to increase the polarity of the transferred solvent and maintain peak shapes in both  $^2Ds$ , analogous to, but different from, ASM used in closed systems [7]. 4) Use of "constructive wraparound", referred to as multi-cycle  $^2D$  chromatography, which is analogous to twin-column recycling chromatography (TCRC) [34–36]. 5) Use of solvent flow rate programming (FRP) to optimize the separation in the  $^2D(2)$  and minimize elution across the edges of  $^2D$  chromatograms. 6) Use of parallel gradients [37,38] on complementary, not orthogonal,  $^2Ds$ . By implementing these innovations combined with LC1MS2 in the  $^1D$  and LC1MS1 in both the  $^2D(1)$  and  $^2D(2)$ , we present here the first report of  $LC1MS2 \times (LC1MS1 + LC1MS1) = LC3MS4$ .

## 2. Materials and methods

### 2.1. Samples and standards

NIST SRM 1849a was obtained from NIST and kept frozen at  $-80$  until extraction. The Certificate of Analysis (COA) indicates

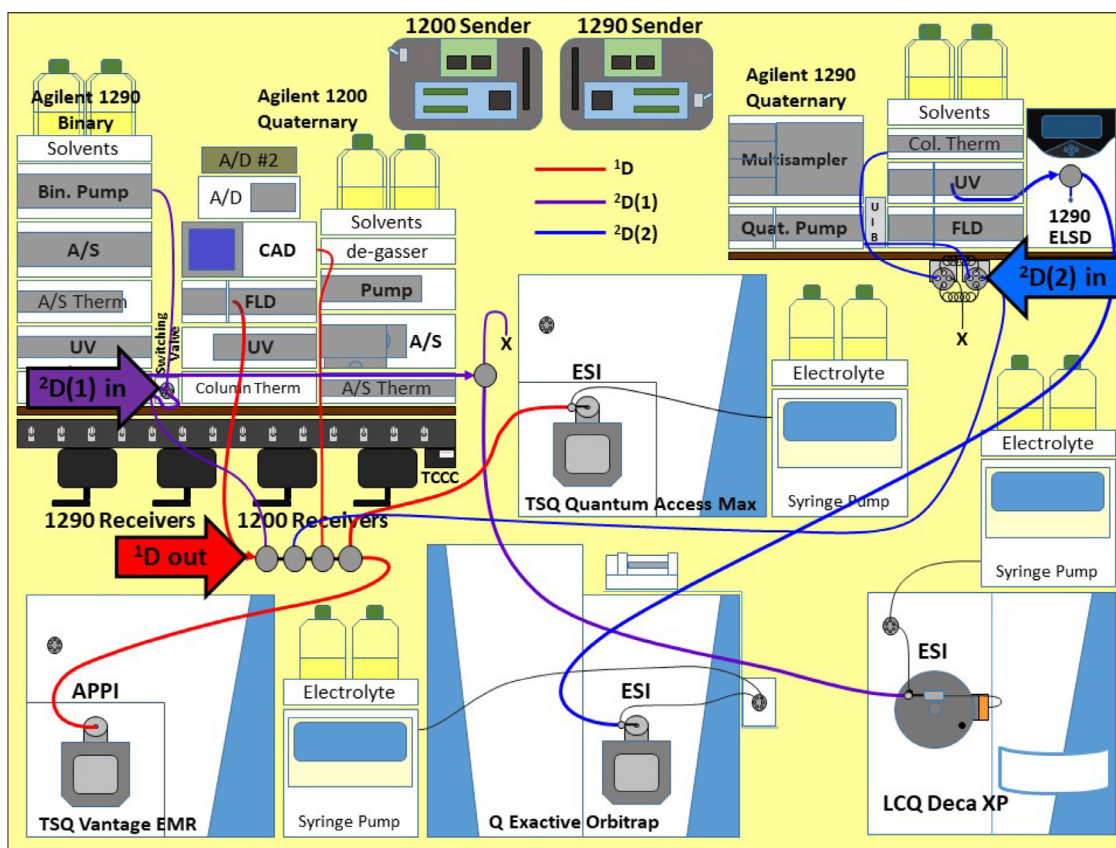


**Fig. 1.** Arrangement of three liquid chromatographs (LCs) and four mass spectrometers plus auxiliary detectors, syringe pumps, and others, for split-flow multi-dimensional liquid chromatography/mass spectrometry (SF-MDLCMS). Coordinated using wireless communication contact closure system (WCCCS) with a Timed Contact Closure Circuit (TCCC) for the 2nd  $^2D$ , or  $^2D(2)$ , switching valves. First dimension (red): Agilent 1200 HPLC, UV, FL, splitter → Corona CAD, APPI-MS, and ESI-MS [= LC1MS2]. Second Dimension #1,  $^2D(1)$  (purple): Agilent 1290 binary UHPLC, UV, FL(opt.), splitter → ELSD, ESI-HRAM-MS [=LC1MS1]; controlled by LC1 2D-LC software. Second Dimension #2,  $^2D(2)$  (blue): Agilent 1290 Infinity Flex II quaternary UHPLC, UV, FL(opt.), splitter → ELSD, ESI-HRAM-MS [=LC1MS1];  $^2D(2)$  valve switching by TCCC controlled from LC3 and WCCCS, LC3 started from LC1 via WCCCS. (For interpretation of the references to colour in this figure legend, the reader is referred to the web version of this article.)

that the certification of SRM 1849a is valid, within the measurement uncertainty specified, until November 30, 2021. Three samples of powder weighing  $\sim 0.6$  g (0.6092 g, 0.5957 g, and 0.6097 g) were added to extraction vessels, and 5 mL of water were added to reconstitute the powder into infant formula, then 4.0 mL of 25.0  $\mu\text{g/mL}$  ergocalciferol (vitamin  $D_2$ ) in chloroform (CF):methanol (MeOH) (2:1) was added as the extraction internal standard (EIS). The samples were extracted using a modification [39] of the method of Folch et al. [40], with minor modifications. Additional details are given in Supplementary Material. After extraction,  $\sim 2$  mL of extract was taken for analysis by gas chromatography (GC) with flame ionization detection (FID) and GC-MS, and the remaining extract was evaporated to dryness under nitrogen. Residue masses of 0.1749 g, 0.1774 g, and 0.1586 g were obtained, respectively. The residues were dissolved in dichloromethane (DCM):MeOH (1:1) and transferred to a 50 mL volumetric flask, but not yet made to the final volume. 4.0 mL of 25.0  $\mu\text{g/mL}$  menaquinone (vitamin  $K_2$ ) were added as the analytical internal standard (AIS), and the solution was made to 50.0 mL, to give final sample concentrations of 3.498 mg/mL, 3.548 mg/mL, and 3.172 mg/mL with 2.00  $\mu\text{g/mL}$  of menaquinone AIS.

Standard stock solutions of 1.0 mg/mL were made in 100 mL amber volumetric flasks and contained retinol (Sigma-Aldrich #95,144, 97.9% pure, St. Louis, MO), retinyl palmitate (#46,959-U, 99.0%),  $\alpha$ -tocopherol (#47,783),  $\delta$ -tocopherol (#47,784),  $\gamma$ -tocopherol (#47,785),  $\alpha$ -tocopheryl acetate (#47,786, 99.9%), vitamin  $D_2$  (#E5750), cholecalciferol (vitamin  $D_3$ ) (#C1357, 98.7%), phylloquinone (vitamin  $K_1$ ) (#47,773, 99.2%), with vitamin  $K_2$

AIS (#47,774). Initial internal standard normalized calculated FSV amounts were adjusted for purity. Working solutions of 25.0  $\mu\text{g/mL}$  were made from the stock solutions, and were further diluted to calibration standard solutions. Because of supplier/delivery issues during the pandemic (e.g., deliveries repeatedly left outside unrefrigerated on hot days) leading to unreliable tocopherol peaks, the internal standard was changed from  $d_6$ - $\alpha$ -tocopherol to menaquinone, vitamin  $K_2$ , and quantification of tocopherols is limited. Calibration standards having the following levels were made: 0.125  $\mu\text{g/mL}$ , 0.250  $\mu\text{g/mL}$ , 0.500  $\mu\text{g/mL}$ , 1.000  $\mu\text{g/mL}$ , 2.500  $\mu\text{g/mL}$ , and 5.000  $\mu\text{g/mL}$ , all containing 1.250  $\mu\text{g/mL}$  of menaquinone AIS.

## 2.2. Liquid chromatography

Due to the fact the LC3MS4 required three LCs and four mass spectrometers plus three auxiliary pumps and six syringe pumps for TED solvents, electrolytes and dopant, each of which need their parameters and chromatographic conditions listed in detail, which takes up many pages, detailed information is provided in the Supplementary Materials, while an overview of instrumentation is provided here. Fig. 1 depicts the combination of three liquid chromatographs (one HPLC, two UHPLC) with detection by four mass spectrometers simultaneously in parallel, with numerous spectral detectors (UV x 3, FL) and spray detectors (ELSD, Corona CAD), referred to as LC3MS4. In the arrangement pictured, there is an HPLC for the  $^1D$ , with flow through the UV and FL detectors, then to a splitter to a Corona CAD and two parallel mass spectrometers, for LC1MS2, as well as two fused silica tub-

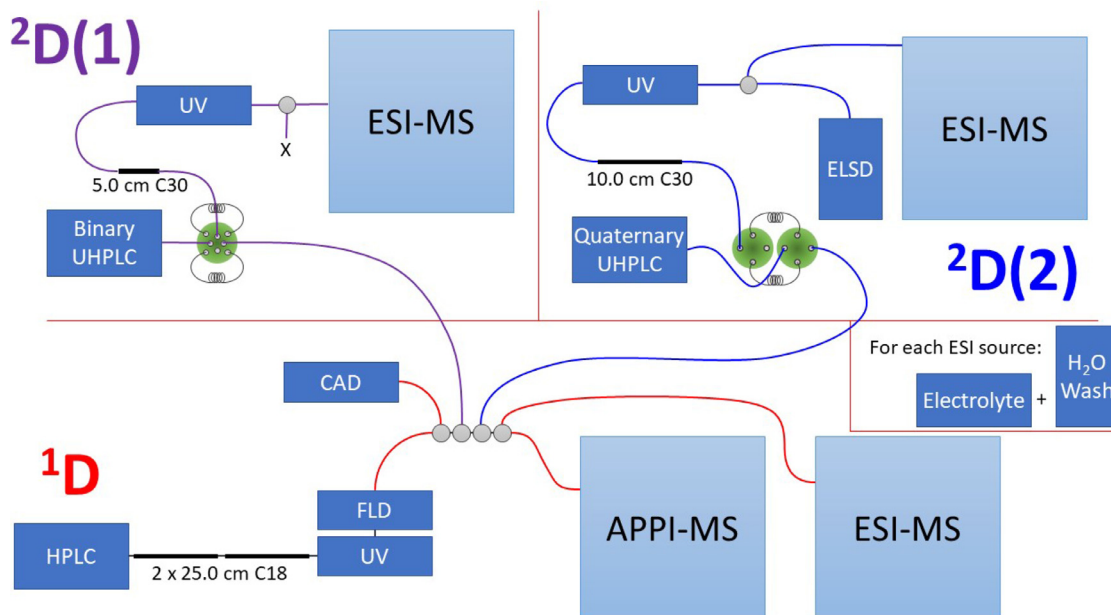


**Fig. 2.** Block diagram of liquid chromatographs and detectors included in LC3MS4 experiments. Some components not shown (i.e., syringe pumps for transferred eluent dilution, dopant, electrolyte, and wash solvents for ESI). See Fig. 1 for additional detail.

ing branches to two parallel second dimension switching valves. Fig. 2 shows a block diagram of the pumps and detectors used in these LC3MS4 experiments. Figs. 1 and 2 show two parallel  $^2\text{D}$ s operating simultaneously in parallel with detection by MS, for  $\text{LC1MS1}_{\text{ESI}} + \text{LC1MS1}_{\text{ESI}}$ , which is combined with the  $^1\text{D}$  to give  $\text{LC1MS2}_{\text{APPI,ESI}} \times (\text{LC1MS1}_{\text{ESI}} + \text{LC1MS1}_{\text{ESI}}) = \text{LC3MS4}$ .

The LC3MS4 system components were coordinated and started or controlled at appropriate times using the wireless communication contact closure system (WCCCS) previously reported [32]. The Timed Contact Closure Circuit (TCCC) was added to the WCCCS to accommodate switching of the  $^2\text{D}(2)$  valves [33]. Relay A in the  $^1\text{D}$  was used as a contact closure that started three of the mass spectrometers ( $2 \times ^1\text{D} + ^2\text{D}(1)$ ), the  $^1\text{D}$  pump started the  $^2\text{D}(2)$  system, and each syringe pump was signaled to refill. Relay A in  $^2\text{D}(2)$  started one mass spectrometer and Relay B started the TCCC via the WCCCS.

The  $^1\text{D}$  HPLC system employed an Agilent 1200 HPLC (Agilent Technologies, Santa Clara, CA, USA) system consisting of a solvent module with membrane degasser (G1379B), quaternary pump (G1311A), autosampler (G1329A) with 1290 thermostat (G1330B) at 15 °C, thermostatted column compartment (G1316A) at 10 °C, diode array detector (DAD) SL (G1315C), 1290 spectra FLD, and ThermoScientific corona CAD attached to two-channel 24-bit analog-to-digital converters (ADCs) for redundancy, an Agilent 35900E and a ThermoScientific SS420X ADC connected to XCalibur software. Two Inertsil ODS-2 columns in series, 25 cm  $\times$  4.6 mm, 5  $\mu\text{m}$  particles (GL Sciences, Torrance, CA, USA) were joined by a circularly bent 7-cm piece of 0.007 in. i.d. stainless steel tubing in the G1316A. The gradient consisted of methanol (MeOH), acetonitrile (ACN), and dichloromethane (DCM) at 1.0 mL/min, with the initial part of the gradient incorporating MeOH for fat-soluble vitamin analysis, followed by a gradient of only ACN and DCM for separation of TAGs. 20  $\mu\text{L}$  of standards and samples were injected. The gradient for the  $^1\text{D}$  is shown in Fig. 3A.

All  $^1\text{D}$  flow went through the non-destructive UVD and FLD, then to a splitter composed of four Valco tees (IDEX Health and Science, Oak Harbor, WA, USA) joined by 10 cm pieces of 0.10" i.d. stainless steel tubing. Flow to each detector was dictated by the length and i.d. of fused silica capillary tubing going to each instru-

ment.  $\sim 150 \mu\text{L}/\text{min}$  was directed to each of two mass spectrometers in the first dimension: a TSQ Vantage EMR (Thermo Scientific, San Jose, CA, USA) operated in atmospheric pressure photoionization (APPI) mode and a TSQ Quantum Access Max in electrospray ionization (ESI) mode.  $\sim 55 \mu\text{L}/\text{min}$  was directed to the  $^2\text{D}(1)$  and  $\sim 65 \mu\text{L}/\text{min}$  was sent to the  $^2\text{D}(2)$ . The remainder of  $^1\text{D}$  eluent,  $\sim 580 \mu\text{L}/\text{min}$ , flowed to the corona CAD.

The  $^2\text{D}(1)$  separation was done on an Agilent 1290 UHPLC system composed of a solvent module with membrane degasser, Infinity binary pump (G4220A), Infinity autosampler (G4226A - disconnected) with FC/ALS Thermostat (G1330B), thermostatted column compartment (G1316C), Infinity diode array detector (DAD) (G4212A), connected through an 8-port, 2-position, 1200 bar column-switching valve (G1170A). The 2D-LC add-on to OpenLab ChemStation C.01.09 was used to control both the  $^1\text{D}$  and  $^2\text{D}(1)$  LCs. The  $^2\text{D}(1)$  separation was done on a 50.0 mm  $\times$  2.1 mm ThermoScientific Accucore C30 column (#27826-052130, ThermoScientific, San Jose, CA) using an ACN:DCM parallel gradient at 1.3 mL/min, in which all analytes eluted in one modulation period, set at 1.91 min. The gradient for the  $^2\text{D}(1)$  is shown in Fig. 3B. The long, narrow-bore 100  $\mu\text{L}$  sample loops of the G1170A valve were replaced with short, wide-bore 200  $\mu\text{L}$  sample loops (Waters, Inc., Milford, MA, USA) to minimize back-pressure and allow for TED. TED solvent was made of 30%  $\text{H}_2\text{O}$ :70% ACN, and was pumped at  $\sim 49 \mu\text{L}/\text{min}$  via an AB 140C syringe pump (Applied Biosystems, obsolete, no longer manufactured).  $^1\text{D}$  flow ( $\sim 55 \mu\text{L}/\text{min}$ ) plus TED solvent flow ( $\sim 49 \mu\text{L}/\text{min}$ ) via a tee attached to the valve inlet gave  $\sim 104 \mu\text{L}/\text{min}$  that filled the 200  $\mu\text{L}$  loops alternately for 1.91 min resulting in  $\sim 99\%$  sample loop fill.

The  $^2\text{D}(2)$  separation was done using an Agilent 1290 Infinity Flex II UHPLC system consisting of a solvent module with membrane degasser, Flexible quaternary pump (G7104A), 1290 Multisampler (G7167A - disconnected), thermostatted column compartment (G7116BC), Infinity diode array detector (DAD) (G7117A), 1260 FLD spectra (G7117B - disconnected), Universal Interface Box (UIB) II (G1390B), and 1290 ELSD (G4261B). The separation was performed using an ACN:DCM gradient on a 100.0 mm  $\times$  3.0 mm ThermoScientific Accucore C30 column (#27,826-103,030, ThermoScientific, San Jose, CA) with a variable flow rate based on

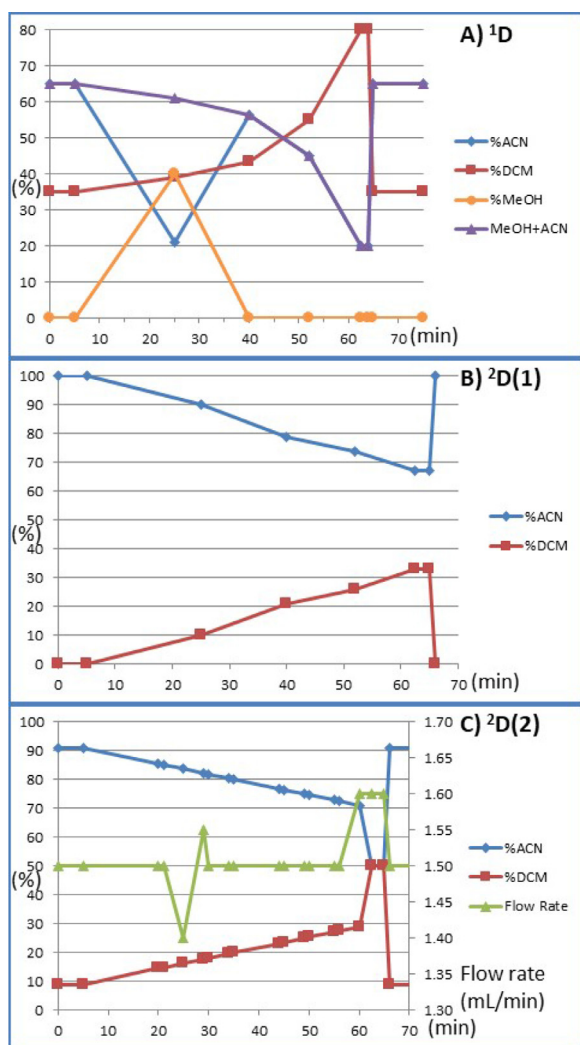


**Fig. 3.** Solvent gradients for three dimensions of separation in LCMS4 experiments. A) <sup>1</sup>D: ACN(+MeOH)/DCM gradient for TAGs 35%/65% → 20%/80% with MeOH for fat-soluble vitamins (FSVs) 0% → 40% → 0%. B) <sup>2</sup>D(1): ACN/DCM 100%/0% → 67%/33%. C) <sup>2</sup>D(2): ACN/DCM 90%/10% → 71%/29% → 50%/50%. Full details given in Supplementary Material.

1.5 mL/min. The gradient for <sup>2</sup>D(2) is shown in Fig. 3C. Analytes remained on column through multiple modulation periods, with the gradient selected such that triolein eluted in the center of the fifth <sup>2</sup>D(2) modulation period after its elution at ~45 min in the <sup>1</sup>D. TED solvent (30% H<sub>2</sub>O:70% ACN) was pumped at ~64 μL/min via an AB 140C syringe pump (Applied Biosystems, obsolete, no longer manufactured) via a tee attached to the valve pair. Two 4-port, two-position UHPLC valves were joined together via the two 250 μL sample loops, and were controlled by the TCCC, which was activated by Relay B of the UIB II, as previously described [33]. <sup>1</sup>D flow (~65 μL/min) plus TED solvent flow (~64 μL/min) gave ~129 μL/min that alternately filled the 250 μL loops for 1.91 min resulting in ~98.5% sample loop fill.

### 2.3. Gas chromatography of fatty acid methyl esters (FAMEs)

Samples were transesterified using 0.5 N sodium methoxide in methanol, according to the method given in Supplementary Materials, and separated on a Supelco (Bellefonte, PA) SP-2560 column, 100 m x 0.25 mm x 0.20 μm film thickness. GC-FID was performed using an Agilent 6890 N instrument. GC-MS was conducted on an Agilent 7890A GC with 5975C MS (in positive-ion CI modes), with

all conditions given in Supplementary Materials. Quantification of FAMEs was done using Agilent OpenLab CDS ChemStation Edition for GC systems, Rev. C.01.05.

### 2.4. Mass spectrometry

The first mass spectrometer that monitored the <sup>1</sup>D was a ThermoScientific TSQ Vantage EMR mass spectrometer operated in APPI mode with a vaporizer temperature of 400 °C. The scan range was limited to *m/z* 150–1150 with a 1 s scan time. Full scans, data-dependent MS/MS, SIM, and SRM scans were obtained for fat-soluble vitamins from 5 to 27 min using the SIM masses and SRM transition masses listed in the Supplementary Materials, along with all other source and operating parameters. Full scans and 2 × data-dependent MS/MS were performed for TAGs from 27 to 75 min. Acetone dopant was supplied via syringe pump at 40 μL/min.

The second mass spectrometer that monitored the <sup>1</sup>D was a ThermoScientific TSQ Quantum Access Max mass spectrometer operated in heated ESI mode at 100 °C. Scans were obtained from *m/z* 150–1150 with a scan time of 1 s. Full scans and 2 × data-dependent MS/MS were performed throughout. An electrolyte mixture of 100 mM NH<sub>4</sub>COOH:MeOH, 1:4, for 20 mM NH<sub>4</sub>COOH, was supplied via syringe pump at 40 μL/min, plumbed through the valve on the front of the instrument, alternating with 0.5% acetic acid in H<sub>2</sub>O supplied via an auxiliary pump at 0.20 mL/min, to flush the source between runs to increase reliability during long sequences of runs, as described previously [41].

The <sup>2</sup>D(1) was monitored using an LCQ Deca XP mass spectrometer operated in ESI mode. Flow was split ~50:50 from the outlet of the 1290 Binary UHPLC system UVD, giving ~0.65 mL/min flow to this instrument, with the remainder to waste. The scan range was *m/z* 150–1150 with alternating MS and data-dependent MS/MS scans. The same electrolyte solution at 40 μL/min and wash solvent at 0.2 mL/min as described for the <sup>1</sup>D above were similarly provided via syringe pump and auxiliary pump, respectively, plumbed into the valve on the front of this instrument as described elsewhere [41].

The <sup>2</sup>D(2), which provided the greatest degree of separation, was monitored using a high-resolution, accurate-mass (HRAM) QExactive orbitrap™ instrument operated in HESI mode, at 100 °C. Resolution was 140,000 for full scans and 70,000 for 2 × data-dependent MS/MS. Electrolyte solution at 20 μL/min and wash solvent at 0.2 mL/min were provided via syringe pump and auxiliary pump, respectively, plumbed into the valve on the side of this instrument [41].

All six syringe pumps (1 × dopant, 3 × electrolyte, 2 × TED solvent) were coordinated to refill after each injection, during the hold-up time, via the WCCCS, using relay A on the Agilent 1200 autosampler as the start signal.

### 2.5. Data analysis

Fat-soluble vitamins were quantified by manual integration of peaks in SIM, SRM, and extracted ion chromatogram (EIC) chromatograms using the Quan Browser program in the ThermoScientific XCalibur workstation software. Results were exported to a Microsoft Excel short report and all quantification calculations were performed using Excel spreadsheets. As we recently reported [42], Agilent ChemStation results should not be used “as-is”, and although Quan Browser results are accurate, the calibration lines and intercepts differ from those obtained from the `linest()` function in Excel by an unexplained factor, so Excel should be used for calculation of all results.

Lipidomic analysis for TAG analysis and quantification was done using ThermoScientific LipidSearch 4.2 applied to the <sup>2</sup>D(2) data.

**Table 1**

Calculated values for fat-soluble vitamins in NIST Standard Reference Material (SRM) 1849a Adult/Infant Formula using APPI-MS extracted ion chromatograms (EICs), selected ion monitoring (SIM), and selected reaction monitoring (SRM).

	SRM Certificate		APPI-MS & MS/MS						Ratio to Min. Std. <sup>b</sup>		
	Cert. Val. <sup>a</sup>	U <sub>95%</sub>	SRM			SIM		EIC		SRM	SIM
$\alpha$ -Tocopheryl Acetate	158	± 18	160.3	± 1.9	152.8	± 4.9	166.8	± 6.6	10.58	11.87	10.84
Retinyl Palmitate	14.30	± 0.20	15.18	± 0.81	13.87	± 0.30	26.89	± 1.87	0.96	1.07	0.98
Free $\alpha$ -Tocopherol	89.20	± 1.9	117.3	± 7.9	150.7	± 18.5	267.2	± 21.3	5.97	6.70	6.12
Retinol (Vitamin A)	7.68	± 0.23	NF <sup>c</sup>	±	NF	±	NF	±	0.51	0.58	0.53
Phylloquinone (Vitamin K1)	1.06	± 0.17	4.43	± 0.07	2.90	± 0.07	-3.06	± 0.36	0.07	0.08	0.07
Cholecalciferol (Vitamin D3)	0.111	± 0.017	5.87	± 0.28	97.46	± 1.35	19.44	± 0.99	0.007	0.008	0.008

<sup>a</sup> Certified value from NIST SRM 1849a Certificate of Analysis, at <https://www-s.nist.gov/srmors/certificates/1849A.pdf>.

<sup>b</sup> Ratio of NIST certified value to lowest calibration standard value (0.125  $\mu$ g/mL), back-calculated using the observed average extraction internal standard and analytical internal standard areas and based on dilution factors and flask volumes.

<sup>c</sup> Not found (NF) at detectable level using primary fragment mass,  $m/z$  269.227.

Due to the relatively long <sup>2</sup>D run times, most peaks eluted in one modulation period, though some eluted in two modulation periods. While this did complicate lipidomic analysis via LipidSearch use of the <sup>2</sup>D(2) data provided the greatest degree of separation of lipids. Peak identities and areas were exported to Excel for calculation of percent relative compositions of TAGs. In cases of intractable overlap of isomers, areas were apportioned using either the relative areas of diacylglycerol-like fragment ions, [DAG]<sup>+</sup>, that were unique to each molecular species or the statistically expected relative amounts based on the GC-FID mole percent composition.

## 2.6. Equivalent carbon number (ECN)

Fatty acids are named by carbon number (C) and degree of unsaturation (U), in the form C:U. The equivalent carbon number (ECN) is  $ECN = C - 2 \times U$ . It is a measure to give information about where a molecule elutes. TAGs cluster by ECN in RP-LC, lowest ECN eluted first, with PUFA TAG within an ECN eluted first, and saturated TAGs last within the same ECN. Some researchers have added other terms to the ECN making it more complicated [43,44], so the basic definition (=C-2 U) is more accurately called the partition number [45], although ECN is more widely used.

## 3. Results and discussion

### 3.1. Fat-soluble vitamins in the <sup>1</sup>D

Although the primary purpose of this report is as the first report of LC3MS4 with three-dimensional chromatography in the form of multi-dimensional LC with two parallel second dimensions, we nevertheless present quantification results of some FSVs here, to demonstrate that we have retained that capability in these SF-CMDLC experiments.

All quantification of FSVs was done using APPI-MS on a tandem sector quadrupole (TSQ) instrument in the <sup>1</sup>D. APPI-MS is a non-contact ionization process, so it did not suffer from the polymerization of ACN on the corona discharge needle of APCI-MS, which leads to loss of sensitivity over the course of a long sequence of runs, as previously mentioned [46]. We obtained data for FSVs using extracted ion chromatograms (EICs) from full-scan data, SIM, and SRM, to compare and contrast the results from each. EICs were expected to produce the least signal, since only 0.001 s of the mass spectrometer's duty cycle is spent at each mass, when scanning at 1000 Da/s ( $m/z$  150–1150 in 1.0 s). Furthermore, EICs are not very specific for each analyte, since any compound having the extracted mass will produce a signal in a given EIC. SIM was expected to be more sensitive (produce more signal), since the scan time was 0.5 s at each SIM mass. But SIM is not entirely specific, since again any compound having the SIM mass produces a signal in the SIM chromatogram. SRM is the most selective, since it requires a precursor

→ product transition, and not all compounds, even if isobaric, produce the same fragments. SRM is also sensitive, but sometimes not as sensitive as SIM, since the MS/MS process is not entirely efficient. To summarize, EICs were expected to be least sensitive and not specific; SIM was expected to be sensitive, but not specific; and SRM was expected to be both sensitive and specific.

The results for all FSVs in SRM 1849a are given in Table 1, even though some were below the limit of detection (LOD) or limit of quantification (LOQ) given in Supplementary Table S-14.  $\alpha$ -Tocopheryl acetate, shown in Fig. 4, was listed as present at a level of  $158 \pm 18$  mg/kg in NIST SRM 1849, and was found at  $160.3 \pm 1.9$  mg/kg by SRM (Fig. 3C),  $152.8 \pm 4.9$  mg/kg by SIM (Fig. 3A) and at  $166.8 \pm 6.6$  mg/kg by EIC, all of which are within the range specified in the COA. The calibration lines by SIM and gave  $r^2$  values of 0.9986 (Fig. 4B) and 0.9975 (Fig. 4D), respectively. Thus, the conventional quantification method used in the <sup>1</sup>D of this 3-D separation was very effective for accurate quantification  $\alpha$ -tocopheryl acetate, even simply using the EIC. Retinyl palmitate gave values of  $15.18 \pm 0.81$  mg/kg by SRM and  $13.87 \pm 0.30$  mg/kg by SIM. The value by SRM was higher than the certified value of  $14.30 \pm 0.20$ , but was within the range of uncertainty in the value by SRM, though not in the uncertainty range for the certified value. The certified value by SIM was slightly lower than the certified value, though the upper range of the value by SIM was well within the certified value range of uncertainty. It was not unexpected that the value by EIC was high, as this is the least specific and thus the least desirable option for quantification at low levels.

The  $\alpha$ -tocopherol peaks in the chromatograms of the NIST SRM 1849a samples were a combination of a sharp peak overlaid by a broad and unresolved background peak. It appears that, since  $\alpha$ -tocopherol acts as an antioxidant, by preferentially being oxidized itself to take the oxidation load off a sample, it may have undergone a combination of oxidation and isomerization over the years of storage, although at  $-80$  °C. Because of the broad sample peaks, it gave larger peak areas, and was difficult to integrate, compared to the sharp, clean peaks of the freshly made calibration standards. Similarly, retinol is well known to be sensitive to degradation, and seems to have been completely decomposed either in the sample or during sample preparation or chromatography. Vitamin K<sub>1</sub> was below the LOQ by SIM, but not by SRM, being present at 0.07–0.08 times the lowest calibration standard (0.125  $\mu$ g/mL). The vitamin K<sub>1</sub> peaks were actually quite well resolved, with good peak shapes, so it is expected that with more replicates and 1/x weighting to compensate for peaks at the very low end of the calibration lines, we may be able to improve the quantification of this FSV. But given that the emphasis here is the first report of LC3MS4, those techniques will be incorporated into future experiments.

Vitamin D<sub>3</sub> was a different matter. Its value was below the LOD and LOQ by SIM, and was present at a level of 0.007 to 0.008 of

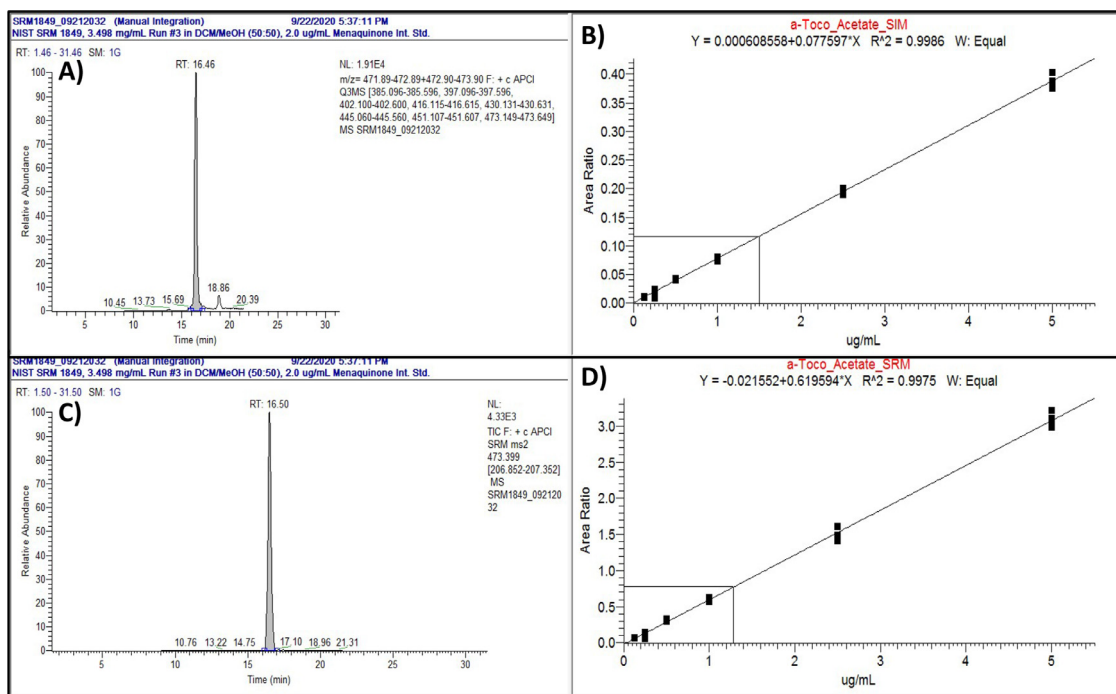


**Fig. 4.** Selected ion chromatogram (SIM) and selected reaction chromatogram (SRM) of  $\alpha$ -tocopheryl acetate in NIST SRM 1849a adult/infant formula as a ratio to menaquinone internal standard by APPI-MS in the first dimension of LC3MS4 experiment. A) SIM chromatogram of  $\alpha$ -tocopheryl acetate at  $m/z$  473.399; B) calibration line by SIM of  $\alpha$ -tocopheryl acetate showing  $r^2 = 0.9986$ ; C) SRM chromatogram of  $\alpha$ -tocopheryl acetate transition at  $m/z$  383.399  $\rightarrow$  269.102; D) calibration line by SRM of  $\alpha$ -tocopheryl acetate showing  $r^2 = 0.9975$ . Values obtained were  $152.8 \pm 4.9$  mg/kg by SIM and  $160.3 \pm 1.9$  mg/kg by SRM, compared to the certified value of  $158 \pm 18$  mg/kg.

the lowest calibration standard ( $0.125 \mu\text{g/mL}$ ). This could not be directly detected at the fortification level of the infant/adult formula. Normally, a dedicated extraction and analysis would be applied, with derivatization for maximum sensitivity by ESI-MS. But even if vitamin D<sub>3</sub> were present at a higher level, its detection in this mixture would be problematic. The presence of a substantial amount of LaCaCy and other isomers that produced abundant  $m/z$  383.3 ( $[\text{CaCa}]^+ = [\text{CyLa}]^+ = [\text{CoM}]^+$ ), gave a substantial  $m/z$  385.3 due to the  $2 \times {}^{13}\text{C}$  isotopic variant overlapping the expected retention time for vitamin D<sub>3</sub>. Since a unit resolution TSQ instrument was used for quantification, it was not able to differentiate the vitamin from the SCFA [DAG]<sup>+</sup> isotope peaks at  $m/z$  385.3.

Nevertheless, quantification of  $\alpha$ -tocopheryl acetate was outstanding, and retinyl palmitate was very close to the certified value (within overlapping uncertainty ranges). This demonstrated that the approach of using vitamin D<sub>2</sub> as the extraction internal standard did adequately compensate for losses during extraction, and vitamin K<sub>2</sub> (menaquinone) was very effective as the analytical internal standard. Thus, while improvements are called for, these data demonstrated that the combined use of an EIS and an AIS in the 1D of the 3-D separation allowed accurate quantification, compared to the conventional 2-D approach of quantification by 'blobs' in the contour plots, which is still problematic.

### 3.2. Gas chromatography with flame ionization detection (GC-FID)

GC-FID results are usually reported as weight percentage composition. Since the FID detector is a carbon mass detector, it makes sense to report in terms of weight percent. Mass spectrometry of TAGs, on the other hand, is a molar relationship to detection, i.e. one charge per molecule per mole of molecules. In MS terms, if we say we have equal amounts of compounds, we mean an equal number of moles of molecules, although the masses of those moles may differ dramatically. In weight% terms, if we say we have equal amounts of FAs, it means equal weights, even though the same

weight of a smaller molecule would contain many more moles. It is imperative to always keep in mind which form of percentage, weight% or mole% is being used, so results can be compared on an equivalent basis. Mole% results are presented in the body of this work, and the weight% values for GC-FID and the NIST SRM 1849a COA values [47] are given in Supplementary Table S-15. The full set of isomers identified is given in Table S-15 by weight% and mole%, since 18:1, 18:2, and 18:3 isomers were each combined in the mole%, in Table 2 (e.g., C18:1 =  $c_9\text{-C18:1} + c_{11}\text{-C18:1} + \text{total trans C18:1}$ ), since these are not distinguished by the LC-MS approach employed.

Table 2 shows the comparison of results from the NIST SRM 1849a Certificate of Analysis [47], converted from weight% to mole%, compared to GC-FID FAME analysis in our lab, also converted from weight% to mole%. The FA in the NIST SRM COA constitute 99.77% of the FA we identified by GC-FID. We identified a few more FA at low% than were reported in the NIST COA, such as C15:0, C17:1, and C20:3, etc.

The absolute and relative differences between our GC-FID FAME results and the certificate results are given in the last two columns of Table 2. According to the certificate: "Values are expressed as  $x \pm U95\%(x)$ , where  $x$  is the certified value and  $U95\%(x)$  is the expanded uncertainty of the certified value. The true value of the analyte is believed to lie within the interval  $x \pm U95\%(x)$  with 95% confidence." Any FAs for which the difference between the GC-FID and certificate mole% FA compositions (Table 2, column 10) is greater than the uncertainty allowed,  $\pm U95\%$  (Table 2, column 3) is not in the true value range of the FA, and so is not in the best, excellent agreement with the NIST SRM COA.

Sixteen of 19 FAs, or 84% of them, gave values that were in the range of the certified values for the NIST SRM COA. Thus, there was excellent agreement between our values and the COA certified values for 16 of 19 FAs. Only three FAs, one reference value (C6:0) and two certified values (C16:1, C18:0) were not in the NIST certified true value range estimates. Since the GC-FID results have

**Table 2**

Comparison of the mole% FA compositions (converted from weight%) from the NIST SRM 1849a Certificate of Analysis (COA) values and from GC-FID, and the mole% FA composition calculated from the LC-ESI-HRAM-MS TAG% composition from lipidomic software analysis, normalized to the NIST SRM Certificate mole% FA and normalized to the GC-FID mole% FA composition.

FA <sup>a</sup>	NIST SRM Certificate		Cert. RF Adj. FA% from TAG%		GC-FID		GC-FID RF Adj. FA% from TAG%		Certificate vs GC-FID Difference	
	FA Mole% <sup>b</sup>	U 95%	FA Mole% <sup>c</sup>	Std. Dev.	FA Mole% <sup>b</sup>	Std. Dev.	FA Mole% <sup>d</sup>	Std. Dev.	Absolute <sup>e</sup>	% Rel. <sup>f</sup>
C6:0	0.46%	0.07%	0.47%	0.06%	0.59%	0.01%	0.59%	0.08%	-0.12%	-25.91%
<b>C8:0<sup>g</sup></b>	4.53%	0.86%	4.55%	0.23%	4.29%	0.06%	4.32%	0.22%	0.23%	5.15%
C10:0	2.96%	0.73%	2.98%	0.23%	2.66%	0.01%	2.67%	0.21%	0.30%	10.24%
C12:0	18.02%	1.26%	18.07%	1.45%	16.94%	0.04%	16.98%	1.39%	1.08%	6.00%
C14:0	5.90%	0.30%	5.92%	0.38%	5.96%	0.01%	5.98%	0.40%	-0.06%	-1.05%
<b>C16:0</b>	7.52%	0.54%	7.56%	0.27%	7.73%	0.02%	7.77%	0.28%	-0.21%	-2.77%
<b>C16:1</b>	0.08%	0.02%	0.08%	0.07%	0.12%	0.00%	0.12%	0.10%	-0.04%	-49.86%
C17:0	0.05%	0.01%	0.05%	0.03%	0.05%	0.00%	0.05%	0.03%	0.00%	-6.40%
<b>C18:0</b>	2.62%	0.15%	2.63%	0.25%	2.82%	0.01%	2.82%	0.26%	-0.19%	-7.32%
<b>C18:1<sup>h</sup></b>	35.66%	3.59%	35.56%	1.40%	36.93%	0.05% <sup>i</sup>	36.82%	1.38%	-1.27%	-3.56%
<b>C18:2<sup>j</sup></b>	18.94%	1.91%	18.93%	0.57%	18.78%	0.03%	18.77%	0.53%	0.16%	0.84%
<b>C18:3<sup>k</sup></b>	2.06%	0.27%	2.06%	0.14%	1.92%	0.01%	1.92%	0.13%	0.14%	6.72%
<b>C20:0</b>	0.24%	0.02%	0.25%	0.03%	0.25%	0.00%	0.25%	0.03%	-0.01%	-3.17%
C20:1	0.21%	0.05%	0.21%	0.02%	0.22%	0.00%	0.22%	0.02%	-0.02%	-8.11%
<b>C20:4</b>	0.37%	0.03%	0.38%	0.06%	0.36%	0.00%	0.36%	0.06%	0.01%	3.27%
<b>C22:0</b>	0.18%	0.02%	0.18%	0.02%	0.19%	0.00%	0.19%	0.02%	-0.01%	-4.43%
<b>C22:6</b>	0.05%	0.01%	NF	NF	0.05%	0.00%	NF	NF	0.00%	2.75%
<b>C24:0</b>	0.10%	0.02%	0.10%	0.08%	0.10%	0.00%	0.10%	0.08%	0.00%	0.99%
<b>C24:1</b>	0.05%	0.01%	0.05%	0.02%	0.05%	0.00%	0.05%	0.02%	0.00%	-4.25%
Sum	100.00%		100.00%		100.00%		100.00%			

<sup>a</sup> Fatty acids given as C:U = Carbon number (CN): Unsaturation (U, number of double bonds).

<sup>b</sup> All weight% compositions converted to mole%. See weight% results for NIST SRM COA FAs in Supplementary Material.

<sup>c</sup> FA mole% calculated from TAG mole% normalized by FA mole% composition from NIST SRM COA.

<sup>d</sup> FA mole% calculated from TAG mole% normalized by FA mole% composition from GC-FID.

<sup>e</sup> Difference between NIST SRM 1849a Certificate FA mole% and GC-FID FA mole%.

<sup>f</sup> Percent relative difference between NIST SRM 1849a Certificate FA mole% and GC-FID FA mole%.

<sup>g</sup> Centered bold values are certified FA% values, others are reference FA% values, from NIST SRM 1849a Certificate of Analysis, at <https://www-s.nist.gov/srmors/certificates/1849A.pdf>.

<sup>h</sup> 18:1 is the sum of cis9-18:1, c11-18:1, all trans18:1 and other isomer.

<sup>i</sup> Uncertainties of combined isomers for 18:1, 18:2, and 18:3 calculated as the uncertainty in the average mole% of combined isomers.

<sup>j</sup> 18:2 is the sum of c9,c12-18:2, c9,t12-18:2, t9,c12-18:2, and other isomer.

<sup>k</sup> 18:3 is the sum of c9,c12,c15-18:3 ( $\alpha$ -Ln) and c6,c9,c12-18:3 ( $\gamma$ -Ln).

such narrow uncertainty values, small differences in absolute values can give values outside the range. For instance, C16:1 is a certified value of  $0.08\% \pm 0.02\%$ , while we obtained a value of  $0.12\% \pm 0.00\%$ . Thus, our value is not in excellent agreement with the certified value, even though it is only 0.02% away from the true value range, 0.06%–0.10%. Similarly, C18:0 has a certified value range of  $2.62\% \pm 0.15\%$ , or 2.47% to 2.77%, while our value of  $2.82\% \pm 0.01\%$  is 0.05% out of the true value range. Finally, C6:0 has a certified value of  $0.46\% \pm 0.07\%$ , or range from 0.39% to 0.53%. Our value of  $0.59\% \pm 0.01\%$  is 0.06% from the true value range, so is also not in excellent agreement.

It is worth noting that the two FAs with the biggest difference between our GC-FID and COA results also had two of the three highest uncertainty ranges, indicating that the contributing labs submitted a wider range of values. Our values for C8:0, C10:0, and C12:0 were all a little too low, whereas our value for C18:1 was too high, though all were still well within the true value ranges. SCFA are well known to be susceptible to losses during extraction, etc., unless precautions are taken (which we took), such as using reduced temperatures.

If all of our values were in the true value ranges of certified and reference values, we would consider that overall excellent agreement. Since 84% of FAs were in excellent agreement with the SRM COA certified or reference values, we consider the overall agreement of our GC-FID results with the certified values and reference values to be very good, but not excellent. These are very good results, especially considering that the NIST values were based on an entirely different extraction and FAME preparation method, targeted specifically at FAMES, while our extraction and FAME analysis was part of a more holistic sample approach, in which we quantified molecules from multiple classes. Thus, our GC-FID FAME com-

position provides a very good, but not excellent, representation of the consensus true composition of NIST SRM 1849a FAs.

In the past, we have always adjusted our TAG compositions to the FA mole% compositions by GC-FID [46,48–50]. In most cases, there is no SRM with certified values available. In the case of SRM 1849a, we have both an analytical GC-FID FAME composition and a certified/reference GC-FID FA% composition. Therefore, we can calculate the response factor adjusted TAG% composition two ways: 1) based on the FA mole% from our values by GC-FID, as normal, and 2) from the NIST certificate FA%. This allows us to compare what the TAG composition would have been if the GC-FID values had been in the center of the true value range for every FA.

The two assumptions that our GC-FID mole FA% response factor calculation approach relies on are: 1) The overall difference in response of TAGs by ESI-MS is due to the chain lengths, degrees of unsaturation, and other factors in the acyl chains of TAGs, which are reflected in the FA composition calculated from the TAG composition (for example, TAG signal by ESI-MS decreases with increasing carbon chain length [51], and signal by ESI-MS increases with increasing degree of unsaturation [51]). 2) Fatty acids are distributed fairly evenly among TAGs.

Special cases where a few TAG species are added to change taste, rheological, or other properties require special treatment [50]. Such special cases give telltale signs in poorer agreement between the GC-FID FA% and the FA% calculated from the TAG%. But in most cases, the FAs are distributed fairly evenly, and the GC-FID FA% and the TAG FA% agree well.

In the present results, there is excellent agreement in Table 2 (cols. 6,8) between the response factor (RF) adjusted FA% calculated from the GC-FID-adjusted TAG% (see “GC-FID RF Adj. TAG%” in Table 3) and the FA% from GC-FID (col. 6). The differ-

**Table 3**

Triacylglycerol (TAG) composition determined from peak integration by lipidomic analysis using LipidSearch 4.2. Un-normalized (raw) percentage composition and compositions normalized to the FA mole% from in-lab GC-FID results and normalized to the converted mole% from the NIST SRM 1849a Certificate of Analysis [28]. The difference represents the effect on TAG% from different FA% normalization approaches.

TAG <sup>a</sup>	C:U <sup>b</sup>	ECN <sup>c</sup>	RT <sup>d</sup>	RT <sup>e</sup>	RT <sup>3</sup>	Unnormalized TAG% <sup>f</sup>		GC-FID Normalized TAG% <sup>g</sup>		SRM Cert. Norm. TAG% <sup>h</sup>		Difference <sup>i</sup>
						Mole%	± SD	Mole%	± SD	Mole%	± SD	
CyCyCa <sup>j</sup>	26:0	26	14.24			0.01%	0.00%	0.01%	0.00%	0.01%	0.00%	0.00%
CoCyLa <sup>j</sup>	26:0	26	14.24			0.06%	0.00%	0.05%	0.00%	0.05%	0.00%	0.00%
CoCaLa <sup>k</sup>	28:0	28	16.3			0.10%	0.01%	0.07%	0.01%	0.07%	0.01%	0.00%
CaCaCy <sup>j</sup>	28:0	28	16.3			0.09%	0.01%	0.07%	0.01%	0.07%	0.01%	0.01%
CyCyLa <sup>k</sup>	28:0	28	16.3			0.27%	0.03%	0.23%	0.03%	0.24%	0.03%	0.01%
CoCyM <sup>k</sup>	28:0	28	16.3			0.02%	0.00%	0.02%	0.00%	0.02%	0.00%	0.00%
CoCoP <sup>l</sup>	28:0	28	16.3			0.00%	0.00%	0.00%	0.00%	0.00%	0.00%	0.00%
LaCoLa <sup>j</sup>	30:0	30	18.51	20.42 [1]		0.64%	0.03%	0.53%	0.03%	0.52%	0.03%	-0.01%
CyCaLa <sup>j</sup>	30:0	30	18.51	20.42 [1]		1.38%	0.07%	1.08%	0.06%	1.16%	0.06%	0.08%
CaCoM <sup>j</sup>	30:0	30	18.51			0.07%	0.01%	0.06%	0.00%	0.05%	0.00%	0.00%
CaCaCa <sup>j</sup>	30:0	30	18.51			0.04%	0.00%	0.03%	0.00%	0.03%	0.00%	0.00%
CaCaLa <sup>j</sup>	32:0	32	20.78			0.97%	0.08%	0.71%	0.06%	0.77%	0.06%	0.07%
LaLaCy <sup>j</sup>	32:0	32	20.78	22.54		4.78%	0.25%	4.02%	0.21%	4.26%	0.22%	0.24%
LaCoM <sup>j</sup>	32:0	32	22.54			0.97%	0.26%	0.80%	0.21%	0.76%	0.20%	-0.04%
LaCyL <sup>l</sup>	38:2	34	22.99			0.11%	0.01%	0.10%	0.01%	0.10%	0.01%	0.00%
LnLnLn <sup>l</sup>	54:9	36	23.64			0.02%	0.01%	0.02%	0.01%	0.02%	0.01%	0.00%
LaCyM <sup>j</sup>	34:0	34	24.95			4.42%	0.36%	3.71%	0.32%	3.84%	0.33%	0.13%
LaCaLa <sup>j</sup>	34:0	34	24.95			3.15%	0.23%	2.50%	0.20%	2.70%	0.21%	0.19%
CaCaM <sup>j</sup>	34:0	34	24.95			0.24%	0.02%	0.17%	0.01%	0.18%	0.01%	0.01%
AdLnAd <sup>l</sup>	58:11	36	25.92			0.02%	0.00%	0.02%	0.00%	0.03%	0.00%	0.00%
AdAdAd <sup>l</sup>	60:12	36	26.13	27.67		0.09%	0.02%	0.17%	0.04%	0.17%	0.04%	0.01%
MMCo <sup>j</sup>	34:0	34	26.80			0.05%	0.01%	0.04%	0.01%	0.04%	0.01%	0.00%
LaCoP <sup>l</sup>	34:0	34	26.80			0.21%	0.06%	0.17%	0.05%	0.17%	0.05%	-0.01%
CaLaL <sup>j</sup>	40:2	36	27.12 [6]			0.03%	0.03%	0.03%	0.03%	0.03%	0.03%	0.00%
MCyL <sup>j</sup>	40:2	36	27.12 [6]			0.04%	0.04%	0.03%	0.03%	0.03%	0.03%	0.00%
CyLaO <sup>l</sup>	38:1	36	27.26			0.70%	0.16%	0.71%	0.16%	0.73%	0.16%	0.01%
LnLnLn <sup>m</sup>	54:8	38	27.70			0.45%	0.05%	0.35%	0.04%	0.37%	0.04%	0.02%
LaCaM <sup>j</sup>	36:0	36	29.00	30.81 [1]		2.16%	0.69%	1.71%	0.55%	1.80%	0.58%	0.09%
LaCyP <sup>l</sup>	36:0	36	29.00	30.81 [1]		1.99%	0.72%	1.67%	0.60%	1.72%	0.62%	0.05%
LaCoS <sup>l</sup>	36:0	36	29.00	30.81 [1]		0.12%	0.04%	0.10%	0.04%	0.10%	0.04%	-0.01%
LaLaLa <sup>j</sup>	36:0	36	29.00	30.81 [1]		2.04%	0.94%	1.75%	0.81%	1.86%	0.86%	0.11%
OCyL <sup>l</sup>	44:3	38	29.45			0.07%	0.01%	0.07%	0.01%	0.07%	0.01%	0.00%
LaLaL <sup>j</sup>	42:2	38	29.59	31.36 [7]		0.09%	0.02%	0.08%	0.01%	0.09%	0.01%	0.00%
MCaL <sup>j</sup>	42:2	38	29.59			0.02%	0.01%	0.02%	0.00%	0.02%	0.00%	0.00%
AdLAd <sup>l</sup>	58:10	38	29.88			0.03%	0.00%	0.05%	0.01%	0.05%	0.01%	0.00%
LLLn <sup>m</sup>	54:7	40	30.36	32.06		2.56%	0.10%	2.12%	0.07%	2.18%	0.08%	0.06%
MCyO <sup>l</sup>	40:1	38	31.32			0.23%	0.02%	0.24%	0.02%	0.24%	0.02%	0.00%
PCoO <sup>j</sup>	40:1	38	31.32			0.03%	0.00%	0.03%	0.00%	0.02%	0.00%	0.00%
CaLaO <sup>l</sup>	40:1	38	31.32			0.39%	0.09%	0.39%	0.09%	0.40%	0.09%	0.01%
LCyP <sup>j</sup>	42:2	38	31.35			0.09%	0.02%	0.07%	0.02%	0.07%	0.02%	0.00%
OCoO <sup>j</sup>	42:2	38	31.35			0.03%	0.01%	0.04%	0.01%	0.03%	0.01%	0.00%
LaLaM <sup>n</sup>	38:0	38	31.55	33.19	33.78 [1]	4.01%	0.85%	3.44%	0.73%	3.57%	0.76%	0.13%
LnOLn <sup>m</sup>	54:7	40	32.06			0.08%	0.01%	0.08%	0.01%	0.08%	0.01%	0.00%
LLaL <sup>l</sup>	48:4	40	32.07			0.02%	0.00%	0.02%	0.00%	0.02%	0.00%	0.00%
LnPLn <sup>m</sup>	52:6	40	32.5	34.07		0.10%	0.02%	0.07%	0.01%	0.08%	0.01%	0.00%
LaCaP <sup>l</sup>	38:0	38	33.19	33.78 [1]		1.28%	0.25%	1.02%	0.20%	1.06%	0.21%	0.05%
LaCyS <sup>l</sup>	38:0	38	33.19	33.78 [1]		1.05%	0.20%	0.91%	0.18%	0.92%	0.18%	0.01%
MCoS <sup>k</sup>	38:0	38	33.23			0.02%	0.01%	0.02%	0.00%	0.02%	0.00%	0.00%
MLaL <sup>j</sup>	44:2	40	34.06			0.13%	0.01%	0.12%	0.00%	0.12%	0.00%	0.00%
PCaL <sup>j</sup>	44:2	40	34.06			0.02%	0.00%	0.02%	0.00%	0.02%	0.00%	0.00%
OCyO <sup>l</sup>	44:2	40	34.06			0.14%	0.01%	0.17%	0.01%	0.17%	0.01%	0.00%
AdOAd <sup>l</sup>	58:9	40	34.27 [6]			0.03%	0.02%	0.04%	0.04%	0.04%	0.04%	0.00%
LLL <sup>l</sup>	54:6	42	34.63	34.95 [1]		5.18%	0.50%	4.55%	0.44%	4.59%	0.45%	0.04%
LnOL <sup>j</sup>	54:6	42	34.66	36.45		1.49%	0.26%	1.49%	0.26%	1.50%	0.26%	0.01%
PCyO <sup>j</sup>	42:1	40	35.63			0.18%	0.03%	0.18%	0.03%	0.18%	0.03%	0.00%
LaLaO <sup>l</sup>	42:1	40	35.63			0.81%	0.07%	0.84%	0.07%	0.86%	0.08%	0.02%
MCoA <sup>l</sup>	42:1	40	35.63			0.10%	0.02%	0.10%	0.02%	0.10%	0.02%	0.00%
MMLa <sup>l</sup>	40:0	40	36.07	37.62		2.04%	0.26%	1.74%	0.22%	1.77%	0.22%	0.02%
LaLaP <sup>m,j</sup>	40:0	40	36.07	37.62		1.38%	0.20%	1.18%	0.17%	1.22%	0.17%	0.04%
AdPAD <sup>l</sup>	56:8	40	36.32			0.09%	0.01%	0.13%	0.02%	0.13%	0.02%	0.00%
OLaL <sup>l</sup>	48:3	42	36.64	38.08 [2]		0.11%	0.02%	0.11%	0.02%	0.11%	0.02%	0.00%
LPLn <sup>l</sup>	52:5	42	36.84	38.47 [6]		1.08%	0.23%	0.89%	0.19%	0.90%	0.19%	0.01%
CaLaS <sup>j</sup>	40:0	40	37.62			0.30%	0.06%	0.25%	0.05%	0.26%	0.05%	0.01%
CyMS <sup>k</sup>	40:0	40	37.62			0.09%	0.01%	0.07%	0.01%	0.07%	0.01%	0.00%
CaCaA <sup>l</sup>	40:0	40	37.62			0.01%	0.00%	0.01%	0.00%	0.01%	0.00%	0.00%
OCaO <sup>l</sup>	46:2	42	38.43	38.54 [3]		0.05%	0.04%	0.06%	0.04%	0.06%	0.04%	0.00%
MML <sup>j</sup>	46:2	42	38.56			0.06%	0.02%	0.05%	0.02%	0.05%	0.02%	0.00%
LLaP <sup>l</sup>	46:2	42	38.56			0.13%	0.04%	0.11%	0.04%	0.11%	0.04%	0.00%
MLaO <sup>l</sup>	44:1	42	38.62	40.19	40.64 [1]	0.63%	0.09%	0.66%	0.09%	0.66%	0.09%	0.00%
LLO <sup>m,j</sup>	54:5	44	39.19	41		6.60%	0.29%	6.96%	0.29%	6.89%	0.29%	-0.07%
OOLn <sup>m,j</sup>	54:5	44	39.19	41	41.53	0.35%	0.09%	0.41%	0.10%	0.41%	0.10%	-0.01%
PCaO <sup>j</sup>	44:1	42	40.19	40.64 [1]		0.09%	0.01%	0.09%	0.01%	0.09%	0.01%	0.00%

(continued on next page)

Table 3 (continued)

TAG <sup>a</sup>	C:U <sup>b</sup>	ECN <sup>c</sup>	RT1 <sup>d</sup>	RT2 <sup>e</sup>	RT3	Unnormalized TAG% <sup>f</sup>		GC-FID Normalized TAG% <sup>g</sup>		SRM Cert. Norm. TAG% <sup>h</sup>		Difference <sup>i</sup>
						Mole%	± SD	Mole%	± SD	Mole%	± SD	
SCyO <sup>j</sup>	44:1	42	40.23			0.02%	0.01%	0.02%	0.01%	0.02%	0.01%	0.00%
LaLaS <sup>j</sup>	42:0	42	40.66	42.22		0.40%	0.06%	0.35%	0.05%	0.36%	0.05%	0.01%
PLaM <sup>j</sup>	42:0	42	40.66	42.22		1.65%	0.16%	1.42%	0.14%	1.43%	0.14%	0.01%
OPLn <sup>j</sup>	52:4	44	41.14	42.8		0.41%	0.07%	0.41%	0.07%	0.41%	0.07%	0.00%
LLP <sup>n,j</sup>	52:4	44	41.14	43.04		4.04%	0.34%	3.53%	0.31%	3.52%	0.31%	-0.01%
LSLn <sup>l</sup>	54:5	44	41.53			0.33%	0.11%	0.28%	0.09%	0.28%	0.09%	0.00%
CaMS <sup>k</sup>	42:0	42	42.22			0.04%	0.01%	0.03%	0.01%	0.03%	0.01%	0.00%
CyPS <sup>k</sup>	42:0	42	42.22			0.00%	0.00%	0.00%	0.00%	0.00%	0.00%	0.00%
OLaO <sup>j</sup>	48:2	44	42.80	43.20		0.17%	0.05%	0.21%	0.06%	0.21%	0.06%	0.00%
PML <sup>j</sup>	48:2	44	43.20			0.12%	0.02%	0.10%	0.01%	0.10%	0.01%	0.00%
LLaS <sup>l</sup>	48:2	44	43.20			0.01%	0.01%	0.01%	0.01%	0.01%	0.01%	0.00%
PLnP <sup>m</sup>	50:3	44	43.49	45.24 [7]		0.10%	0.02%	0.08%	0.01%	0.08%	0.01%	0.00%
LMaL <sup>l</sup>	53:4	45	43.61 [7]			0.04%	0.02%	0.04%	0.02%	0.04%	0.02%	0.00%
LLG <sup>l</sup>	56:5	46	43.88			0.08%	0.01%	0.08%	0.01%	0.08%	0.01%	0.00%
PLaO <sup>j</sup>	46:1	44	43.88	44.98 [5]		0.44%	0.10%	0.46%	0.10%	0.46%	0.10%	0.00%
MMO <sup>j</sup>	46:1	44	43.88	44.98 [5]		0.14%	0.05%	0.15%	0.05%	0.15%	0.05%	0.00%
OLO <sup>n</sup>	54:4	46	44.09	45.54		7.37%	1.04%	9.07%	1.22%	8.85%	1.20%	-0.22%
OCaS <sup>j</sup>	46:1	44	44.89 [7]			0.01%	0.01%	0.01%	0.01%	0.01%	0.01%	0.00%
OOPo <sup>j</sup>	52:3	46	46.01	47.03 [1]		0.05%	0.04%	0.17%	0.14%	0.13%	0.11%	-0.04%
LSL <sup>m</sup>	54:4	46	46.15	47.95		1.28%	0.25%	1.14%	0.22%	1.12%	0.22%	-0.02%
ALLn <sup>l</sup>	56:5	46	46.56 [7]			0.01%	0.01%	0.01%	0.01%	0.01%	0.01%	0.00%
OPL <sup>l</sup>	52:3	46	46.64	46.98		3.57%	0.33%	3.74%	0.33%	3.67%	0.33%	-0.08%
PCaS <sup>l</sup>	44:0	44	46.87 [7]			0.04%	0.01%	0.04%	0.00%	0.04%	0.00%	0.00%
MPM <sup>j</sup>	44:0	44	47.00			0.19%	0.02%	0.16%	0.02%	0.16%	0.02%	0.00%
MLaS <sup>j</sup>	44:0	44	47.00			0.30%	0.04%	0.26%	0.04%	0.26%	0.04%	0.00%
LaLaA <sup>l</sup>	44:0	44	47.00			0.02%	0.00%	0.01%	0.00%	0.01%	0.00%	0.00%
PPLa <sup>l</sup>	44:0	44	47.00			0.36%	0.04%	0.31%	0.04%	0.31%	0.04%	0.00%
OMO <sup>l</sup>	50:2	46	47.64			0.23%	0.09%	0.28%	0.11%	0.28%	0.11%	-0.01%
OSLn <sup>j</sup>	54:4	46	47.95			0.16%	0.09%	0.16%	0.09%	0.16%	0.09%	0.00%
PLP <sup>n</sup>	50:2	46	49.64	51.56 [5]		0.90%	0.08%	0.78%	0.07%	0.77%	0.07%	-0.01%
OLaS <sup>l</sup>	48:1	46	49.78	51.30		0.09%	0.07%	0.10%	0.07%	0.09%	0.07%	0.00%
OMP <sup>l</sup>	48:1	46	49.78	51.30		0.27%	0.08%	0.28%	0.08%	0.28%	0.08%	-0.01%
SPLn <sup>l</sup>	52:3	46	50.01			0.06%	0.01%	0.05%	0.01%	0.05%	0.01%	0.00%
OMaL <sup>l</sup>	53:3	47	50.1 [7]			0.04%	0.02%	0.05%	0.03%	0.05%	0.02%	0.00%
OLC <sup>l</sup>	56:4	48	50.39			0.12%	0.02%	0.14%	0.02%	0.14%	0.02%	-0.01%
OOO <sup>l</sup>	54:3	48	50.55	52.06	54.79 [3]	9.72%	0.36%	13.67%	0.47%	13.20%	0.46%	-0.47%
LAL <sup>m</sup>	56:4	48	52.74	55.45 [2]		0.08%	0.02%	0.07%	0.02%	0.07%	0.02%	0.00%
BLLn <sup>l</sup>	58:5	48	53.16 [6]	53.98 [2]		0.01%	0.02%	0.02%	0.02%	0.02%	0.02%	0.00%
MaPL <sup>l</sup>	51:2	47	53.64 [7]			0.01%	0.01%	0.01%	0.01%	0.01%	0.01%	0.00%
LSO <sup>l</sup>	54:3	48	54.07	56.73 [1]		1.30%	0.64%	1.39%	0.68%	1.35%	0.66%	-0.04%
OOP <sup>n</sup>	52:2	48	54.13	55.7 [7]	58.14 [1]	3.98%	0.38%	4.88%	0.48%	4.72%	0.46%	-0.16%
PLaS <sup>k</sup>	46:0	46	54.59 [5]			0.16%	0.02%	0.14%	0.02%	0.14%	0.02%	0.00%
MLaA <sup>k</sup>	46:0	46	54.59 [5]			0.01%	0.00%	0.01%	0.00%	0.01%	0.00%	0.00%
PPM <sup>k</sup>	46:0	46	54.59 [5]			0.10%	0.02%	0.08%	0.02%	0.08%	0.02%	0.00%
LPS <sup>l</sup>	52:2	48	57.65	59.49 [5]	59.73 [1]	0.57%	0.04%	0.51%	0.03%	0.49%	0.03%	-0.02%
OOG <sup>l</sup>	56:3	50	58.64	59.51 [5]		0.26%	0.04%	0.36%	0.05%	0.34%	0.05%	-0.02%
OMS <sup>l</sup>	50:1	48	59.09 [7]	61.86 [2]		0.03%	0.03%	0.03%	0.03%	0.03%	0.03%	0.00%
POP <sup>m,j</sup>	50:1	48	59.17	61.86 [2]		0.62%	0.11%	0.65%	0.11%	0.63%	0.11%	-0.02%
OMaO <sup>l</sup>	53:2	49	59.46 [7]			0.04%	0.02%	0.05%	0.03%	0.05%	0.03%	0.00%
LLB <sup>l</sup>	58:4	50	60.42	61.58		0.07%	0.02%	0.10%	0.03%	0.10%	0.03%	0.00%
LMaS <sup>l</sup>	53:2	49	61.15 [7]			0.01%	0.00%	0.01%	0.00%	0.01%	0.00%	0.00%
GPO <sup>l</sup>	54:2	50	61.4 [7]	62.04 [1]		0.03%	0.03%	0.04%	0.04%	0.04%	0.03%	0.00%
LOA <sup>l</sup>	56:3	50	61.46			0.18%	0.07%	0.20%	0.08%	0.20%	0.08%	0.00%
LSG <sup>j</sup>	56:3	50	61.46			0.01%	0.00%	0.01%	0.01%	0.01%	0.00%	0.00%
BOLn <sup>j</sup>	58:4	50	61.58			0.01%	0.01%	0.02%	0.01%	0.02%	0.01%	0.00%
OOS <sup>n</sup>	54:2	50	61.59	62.06 [7]		1.75%	0.15%	2.18%	0.18%	2.08%	0.17%	-0.09%
SSLa <sup>l</sup>	48:0	48	62.02			0.01%	0.00%	0.01%	0.00%	0.01%	0.00%	0.00%
SMP <sup>l</sup>	48:0	48	62.02			0.08%	0.02%	0.07%	0.01%	0.07%	0.01%	0.00%
APL <sup>l</sup>	54:2	50	62.36	62.63 [5]		0.05%	0.02%	0.05%	0.02%	0.04%	0.02%	0.00%
OLN <sup>l</sup>	60:4	52	62.41			0.03%	0.00%	0.04%	0.01%	0.04%	0.01%	0.00%
SSL <sup>m</sup>	54:2	50	62.71			0.12%	0.04%	0.11%	0.04%	0.10%	0.03%	0.00%
POS <sup>l</sup>	52:1	50	62.76	63.15 [7]		0.41%	0.02%	0.43%	0.02%	0.42%	0.02%	-0.02%
LLLg <sup>l</sup>	60:4	52	62.95			0.02%	0.00%	0.05%	0.00%	0.05%	0.00%	0.00%
LOB <sup>l</sup>	58:3	52	63.05	63.09 [3]		0.11%	0.01%	0.16%	0.01%	0.16%	0.01%	0.00%
OOA <sup>n</sup>	56:2	52	63.25			0.33%	0.02%	0.42%	0.03%	0.41%	0.03%	-0.01%
OON <sup>l</sup>	60:3	54	63.85	64.48 [6]		0.07%	0.04%	0.11%	0.06%	0.10%	0.06%	0.00%
PPS <sup>l</sup>	50:0	50	64.35			0.02%	0.01%	0.02%	0.01%	0.02%	0.01%	0.00%
SLA <sup>l</sup>	56:2	52	64.40			0.02%	0.01%	0.02%	0.01%	0.02%	0.01%	0.00%
LPB <sup>l</sup>	56:2	52	64.40			0.04%	0.01%	0.05%	0.01%	0.05%	0.01%	0.00%
POA <sup>l</sup>	54:1	52	64.44			0.05%	0.02%	0.06%	0.02%	0.05%	0.02%	0.00%

(continued on next page)

Table 3 (continued)

TAG <sup>a</sup>	C:U <sup>b</sup>	ECN <sup>c</sup>	RT1 <sup>d</sup>	RT2 <sup>e</sup>	RT3	Unnormalized TAG% <sup>f</sup>		GC-FID Normalized TAG% <sup>g</sup>		SRM Cert. Norm. TAG% <sup>h</sup>		Difference <sup>i</sup>
						Mole%	± SD	Mole%	± SD	Mole%	± SD	
SOS <sup>n,j</sup>	54:1	52	64.44			0.09%	0.03%	0.10%	0.04%	0.10%	0.03%	-0.01%
LOL <sup>g,l</sup>	60:3	54	64.47 [7]			0.05%	0.06%	0.11%	0.12%	0.11%	0.12%	0.00%
<b>Sum</b>						100.00%		100.00%		100.00%		

<sup>a</sup> Names are listed as the most abundant regioisomer, based on fragment ratios in mass spectra. The following FA common names and nomenclature were used: Co: C6:0 = caproic acid; Cy: C8:0 = caprylic; Ca: C10:0 = capric; La: C12:0 = lauric; M: C14:0 = myristic; P: C16:0 = palmitic; Po: C16:1 = palmitoleic; S: C18:0 = stearic; O: *cis* (c)9-C18:1 = oleic (includes isomers: c11-C18:1 = vaccenic, *trans* (t)-C18:1); L: c9,c12C18:2 = linoleic (includes isomers: c9,t12-18:2, and t9,c12-18:2); Ln: c9,c12,c15-C18:3 = linolenic (includes isomer c6,c9,c12-18:1 = gamma linolenic,  $\gamma$ -Ln); A: C20:0 = arachidic; G: C20:1 = gadoleic; B: C22:0 = behenic; E: C22:1 = erucic; Lg: C24:0 = lignoceric; N: C24:1 = nervonic acid. Isomers combined in LC-MS results.

<sup>b</sup> C:U = Carbon number (CN): Unsaturation (U, number of double bonds).

<sup>c</sup> ECN = Equivalent carbon number = CN - (2 x U) = carbon number - 2 x number of sites of unsaturation.

<sup>d</sup> Retention times, RT, are mean RTs across 8 of 9 runs (1st run excluded from average RT). Numbers in [] indicate the number of observations out of 8 runs. Peaks could split into two modulation periods, with isomers extending to a third modulation period.

<sup>e</sup> Number in brackets is number of replicate runs RT observed.

<sup>f</sup> Unnormalized TAG% is the average composition of raw areas from peak integration of all 9 runs without application of any response factors. SD is the  $\sqrt{SD_1^2 + SD_2^2 + SD_3^2}$  for the three samples in triplicate.

<sup>g</sup> GC-FID Normalized TAG% is the TAG% normalized to GC-FID-derived FA response factors (RFs). SD is the  $\sqrt{SD_1^2 + SD_2^2 + SD_3^2}$  for the three samples in triplicate.

<sup>h</sup> SRM Cert. Norm. TAG% is the TAG% normalized using FA RFs from the mole% FA composition obtained from the weight% FA composition reported in the NIST SRM 1849a Certificate of Analysis [28]. SD is the  $\sqrt{SD_1^2 + SD_2^2 + SD_3^2}$  for the three samples in triplicate.

<sup>i</sup> Difference in TAG% from using FA RFs calculated from the NIST SRM 1849a Certificate of Analysis FA composition versus from the GC-FID.

<sup>j</sup> Regioisomer determined from Critical Ratio 2 of apportioned TAGs.

<sup>k</sup> Regioisomer not defined.

<sup>l</sup> Regioisomer determined from Critical Ratios of pure peaks.

<sup>m</sup> Regioisomer assigned from literature values (Holcapek et al. 2010), Ref. [44].

<sup>n</sup> Regioisomer assigned by comparison to regioisomer standards.

ence between the GC-FID FA% and the TAG FA% is less than (usually much less than) the uncertainty in the TAG FA% for every FA except DHA (C22:6). The main difference between the two FA% compositions is the fact that the lipidomics software did not identify any DHA-containing TAGs in Table 3, so we report a DHA% of “not found”, “NF”, whereas GC-FID was able to identify DHA at 0.05%. Of course, the 0.05% total of DHA would be spread across all DHA TAG molecular species, so each TAG would be present at a fraction of that level, making them harder to detect by LC-MS. Table 2 shows that our response factor adjustment approach based on GC-FID/LC-MS response factors gave a FA mole% composition from the TAG% composition that is in excellent agreement with the results obtained by GC-FID.

Alternatively, we could choose to use the NIST SRM COA FA mole% to produce response factors, to adjust the TAG composition to the COA FA composition. The “SRM Cert. RF Adj. TAG%” composition thus obtained is also given in Table 3. The FA mole% that comes from that SRM certificate RF adjusted TAG% is given in Table 2 as the “Cert. RF Adj. FA% from TAG%”. As expected, the agreement of the FA% from the certificate-adjusted TAG% with the NIST SRM COA composition is excellent. The difference between the FA mole% calculated from the certificate-adjusted TAG% is small, mostly much smaller than the uncertainty in the certificate values.

These FA mole% composition results show that the Byrdwell method [46,50,52,53] for GC-FID/LC-MS response factors produces a TAG% composition that yields a FA% composition in excellent agreement with the GC-FID FAME results. Our approach compensates for the overall over-response or under-response of the FAs due to chain length and degree of unsaturation, but the relative differences between TAGs remains, giving a composition of TAGs that reflects TAG molecular species differences, while still conforming to the overall FA response reflected in the FA mole%. In summary, there was very good, but not quite excellent, agreement between the FA mole% determined by GC-FID in our lab and the NIST SRM COA values. And there was excellent agreement in both cases of calculating response factors for TAGs from the GC-FID results or the NIST SRM COA values. Either way, the appropriately adjusted

TAG% composition gave excellent agreement to the FA% composition used to calculate response factors, while still reflecting TAG molecular species differences determined by LC-MS.

### 3.3. Triacylglycerols in the <sup>1</sup>D

Previously [25], we employed a 54 min gradient from which all acetonitrile had been removed, because the <sup>2</sup>D employed a silver ion column for which ACN was the strong eluent. That method was comprised mostly of MeOH, then DCM with an increasing gradient of EtOH to separate and elute fat-soluble vitamins, followed by increasing EtOH to elute TAGs. Full-length runs for separations of TAGs were 130 min, while runs for FSV calibration standards were 54 min.

In the present analysis, we used NIST SRM 1849 as preparation for analysis of milk, which contains many saturated TAGs, none of which are substantially retained by silver-ion chromatography, and many of which contain very short-chain (2–12 carbon) FAs. Therefore, we went back to the ACN/DCM gradient similar to what we previously used [46], to get the best resolution in the <sup>1</sup>D possible. Then, to make the analysis shorter and more useful for higher throughput analyses, we shortened the gradient to 65 min, with a 10 min recycle time. Here we performed a gradient in MeOH, which was required for FSV elution, under the first part of the ACN/DCM gradient by replacing ACN with MeOH (Fig. 3A, orange line vs. blue line). Thus, we were able to reduce the run times to 65 min with a 10 min re-equilibration time, for 75 min for TAGs, while still separating FSVs. The runs for FSV calibration standards were reduced from 54 min [25] to 27 min.

*APPI-TSQ-MS in the <sup>1</sup>D.* Previously, we have always used quantification by extracted ion chromatograms (EICs), such as those in Figs. 5 and 6, and XCalibur Quan Browser workstation software to quantify TAGs by APCI-MS, APPI-MS and ESI-MS. We used EICs of diacylglycerol (DAG)-like fragments, [DAG]<sup>+</sup>, to visualize what FAs were present in the TAGs, and use the masses of the EICs of [DAG]<sup>+</sup> and [M+H]<sup>+</sup> or [M+NH<sub>4</sub>]<sup>+</sup> ions for integration of peaks in Quan Browser. However, as the number and complexity of samples has increased, we have had to move away from manual integration

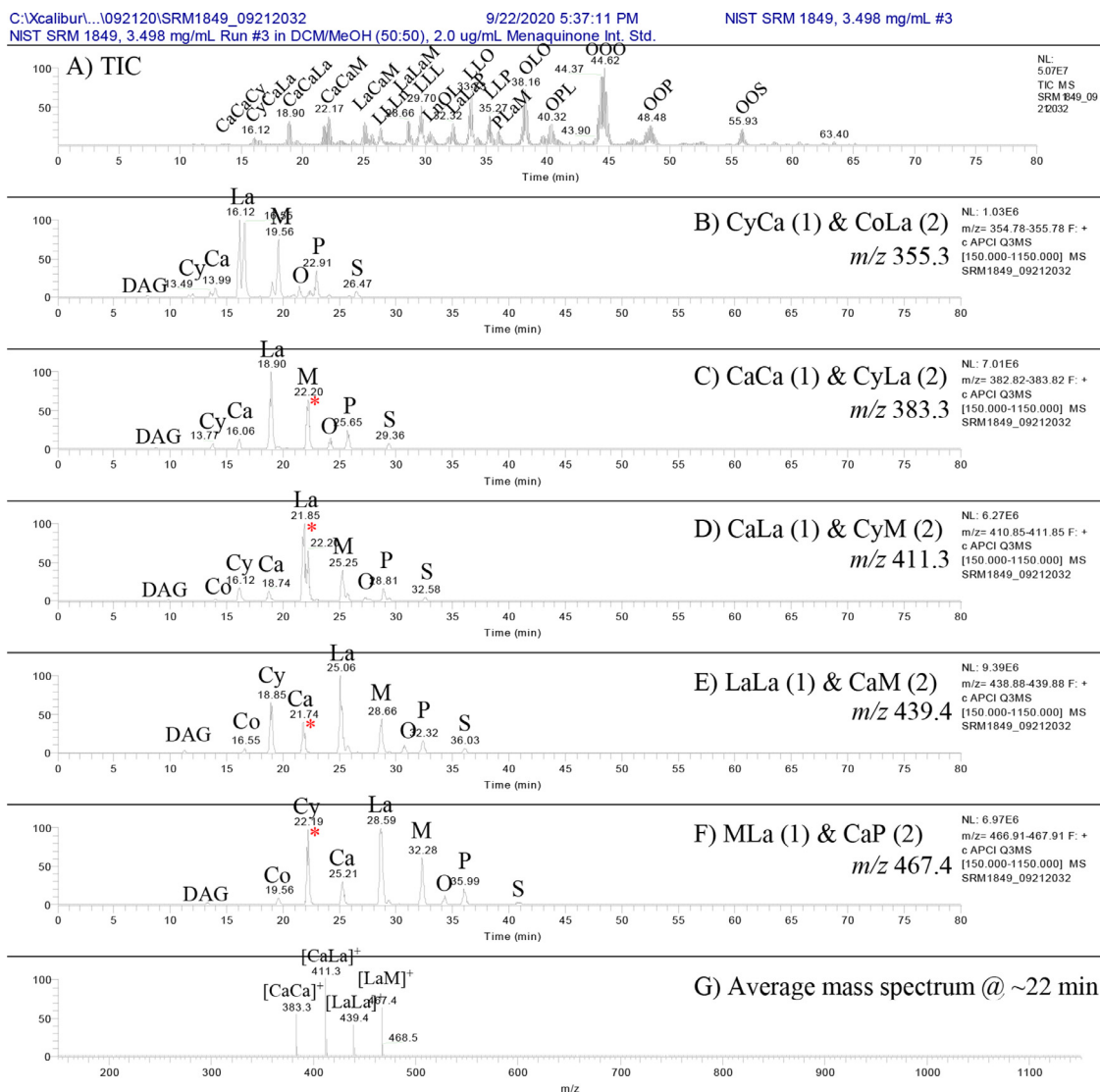


**Fig. 5.**  $^1\text{D}$  Total ion chromatogram (TIC) and extracted ion chromatograms (EICs) of diacylglycerol-like fragments,  $[\text{DAG}]^+$ , of short-chain fatty acid (SCFA) containing TAGs, by APPI-MS.

of the large number of peaks in the current dataset. Therefore, a lipidomics approach is demonstrated here to obtain the mass spectral fragment intensities necessary to calculate the CRs. Identification and quantification of TAGs was done using ESI-HRAM-MS attached to the  $^2\text{D}(2)$  data, so the  $^1\text{D}$  data were used for qualitative purposes only, assisting in peak identification.

The EICs in Figs. 5 and 6 of the  $^1\text{D}$  separation for one replicate show several of the overall trends observed in the TAG compositions quantified in the  $^2\text{D}(2)$ . They demonstrate that the short-chain fatty acid (SCFA, C6-C14) TAGs have  $[\text{DAG}]^+$  fragments with other SCFA, but not as much with medium/long-chain FAs (MLCFAs, C16-C24), specifically O (C18:1), P (C16:0), and S (C18:0). And MLCFA TAGs similarly were in TAGs with other MLCFAs, but not with SCFAs. If this were an inter-esterified or natural mixture, a large number of statistically expected combinations of all FAs with all other FAs would be expected. These chromatograms show a mixture of SCFA TAGs and MLCFA TAGs, without the classes being thoroughly intermingled. For instance, in Fig. 6 the oleic FA peak is the largest in each EIC, whereas in SCFA-TAGs the "O" peak in each EIC is one of the smallest peaks. The amount of oleic acyl chains in the SCFA-TAG fraction is clearly smaller than in the MLCFA-TAG fraction. These observations are consistent with the fact that this

is a formulated product composed of different TAG portions. Nevertheless, within the sub-groups, SCFA TAGs and MLCFA TAGs, the FA were distributed rather evenly (seen in the similar appearances of EICs of different  $[\text{DAG}]^+$  fragments, e.g., Figs. 5E, F). Therefore, within sub-groups, statistically expected  $[\text{DAG}]^+$  abundances based on the GC-FID FA mole% could still be used to apportion a few intractably overlapped abundances.

Patterns of elution can be seen in the  $^1\text{D}$  that become even more clear in the  $^2\text{D}(2)$ . Sequentially viewing mass spectra in a  $^1\text{D}$  peak, or "stepping across" the peaks revealed patterns in the elution. The first thing to notice in Supplementary Figures 6D to 6F is the long-known trend [54] that saturated TAGs give little or no  $[\text{M}+\text{H}]^+$  by APCI- and APPI-MS [55]. Therefore, TAGs were identified manually by a combination of the  $[\text{DAG}]^+$  in APPI-MS spectra combined with the  $[\text{M}+\text{NH}_4]^+$  by ESI-MS, such as Fig. 7C, in parallel at the same RT.

The most homogeneous SCFA-TAG eluted first, which were those having FA chains the same or similar lengths, such as LaLaLa in Fig. S-5D. Then, the next more heterogeneous SCFA-TAG eluted, with a greater disparity between FA chain lengths, such as CaLaM in Fig. S-5E. Then, the most heterogeneous isomer eluted, with the greatest disparity between FA chains, such as CyLaP in Fig. S-5F.

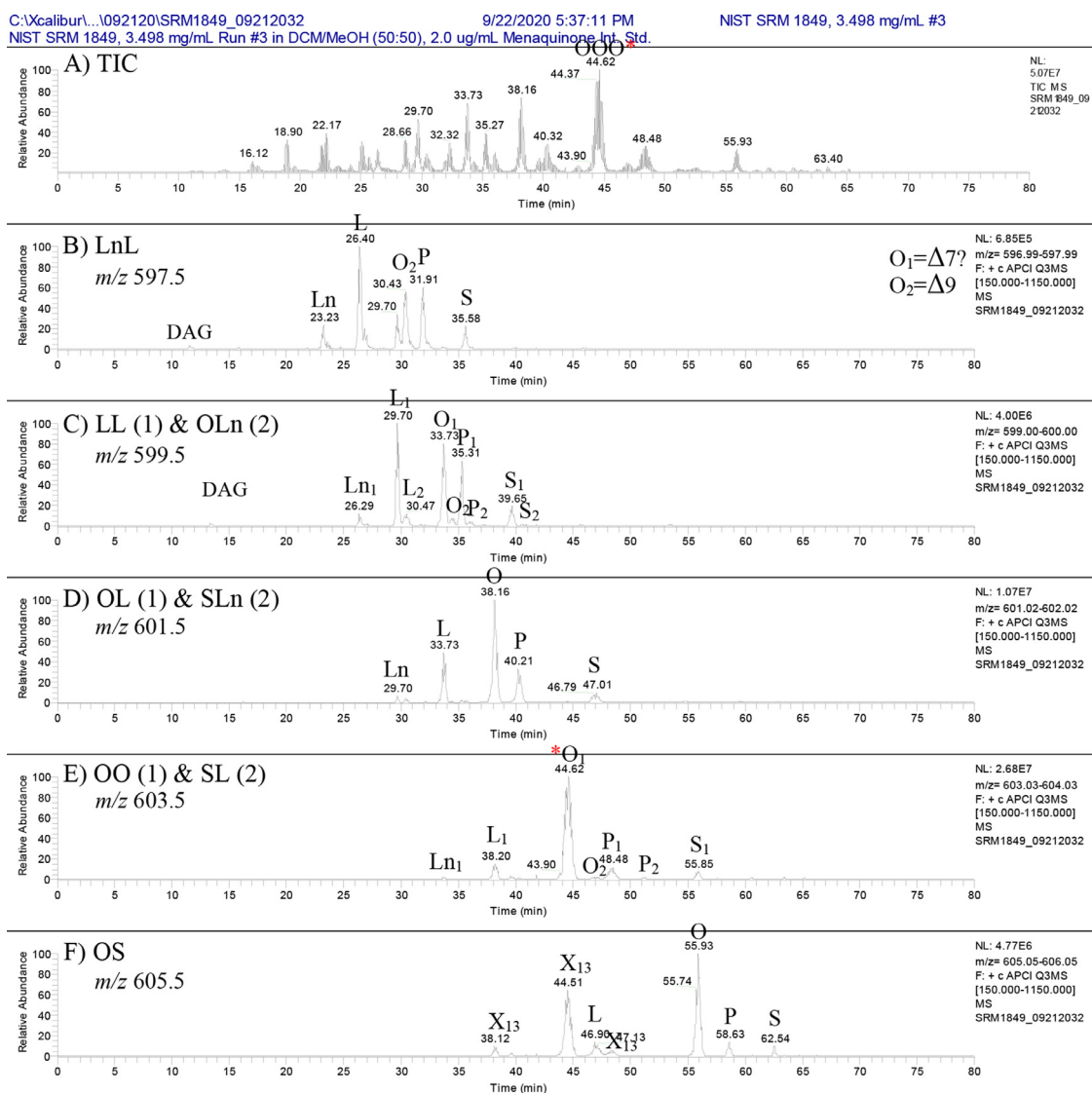


**Fig. 6.** <sup>1</sup>D Total ion chromatogram (TIC) and extracted ion chromatograms (EICs) of diacylglycerol-like fragments, [DAG]<sup>+</sup>, of medium-chain fatty acid (MCFA) containing TAGs, by APPI-MS. See Fig. 1 for TIC peak identities. X13 is the 2 x <sup>13</sup>C isotopic variant of TAG having one more site of unsaturation.

The APPI-MS data produced abundant diacylglycerol-like fragment ions, [DAG]<sup>+</sup>, such as in Fig. 5G, and not [M+H]<sup>+</sup>, which the lipidomics software incorrectly identified as intact diacylglycerol molecules, and was not able to identify TAGs from the [DAG]<sup>+</sup> fragments. LipidSearch only searches for protonated molecules and adduct ions in full-scan spectra, and only recognizes [DAG]<sup>+</sup> fragments in MS/MS spectra. When [DAG]<sup>+</sup> fragments were abundant in full-scan spectra, LipidSearch treated those as independent protonated molecules, [M+H]<sup>+</sup>, giving a false list of diacylglycerols, and identifying few or no intact SCFA, because saturated TAGs produced no intact [M+H]<sup>+</sup>, as long-reported for APCI-MS [54] and APPI-MS [55].

**ESI-TSQ-MS in the <sup>1</sup>D.** The first dimension, <sup>1</sup>D, LC-ESI-MS total ion current chromatogram (TIC) of NIST SRM 1849a is shown in Fig. 7. Normally, we use ESI-MS in the <sup>1</sup>D for identification and quantification of TAGs [41,46]. However, the auto-tune of the instrument obtained prior to these experiments had a higher than normal capillary voltage, which caused up-front fragmentation without that feature being explicitly activated. This caused the presence of [DAG]<sup>+</sup> fragments in full-scan ESI-MS spectra such as Fig. 7C, confusing the software, as mentioned above for APPI-MS. Whether in ESI-MS or APPI-MS mass spectra, the presence of

[DAG]<sup>+</sup> fragments rendered the <sup>1</sup>D ESI-MS data essentially unusable for LipidSearch software.

Nevertheless, the unit-resolution <sup>1</sup>D ESI-MS data were highly valuable for identification of the SCFA-TAGs, since these produced abundant [M+NH<sub>4</sub>]<sup>+</sup> adducts, Figs. 7D-F, that allowed easy identification of the TAG molecular weights. Also, ESI-MS was more sensitive than APPI-MS, so the chromatogram in Fig. 7A has more visually identifiable features than in Figs. 5A, 6A. Fig. 7C shows an average ESI-MS mass spectrum across the pair of peaks at 25 to 26 min, and Figs. 7D-F show average mass spectra over partial ranges of those peaks. The front peak exhibits mostly the spectrum in Fig. 7D, which indicates LaLaLa from the [LaLa]<sup>+</sup> and [M+NH<sub>4</sub>]<sup>+</sup> ions. After the peak maximum at 25.07 min (Fig. 7B), the mass spectrum in Fig. 7E becomes dominant, indicating the appearance of LaCaM, proved by the presence of [LaCa]<sup>+</sup>, [CaM]<sup>+</sup> (= [LaLa]<sup>+</sup>), and [LaM]<sup>+</sup> with the [M+NH<sub>4</sub>]<sup>+</sup> at  $m/z$  656.6. The next partially unresolved neighboring isomer elutes at 25.72 min, and gives the average mass spectrum in Fig. 7F, which indicates LaCyP, based on the presence of [LaCy]<sup>+</sup>, [CyP]<sup>+</sup>, and [LaP]<sup>+</sup>, with the continued [M+NH<sub>4</sub>]<sup>+</sup> at  $m/z$  656.6.

Sequentially viewing mass spectra in unresolved peaks, or “stepping across” the peaks, revealed the pattern in the elution.

The most homogeneous SCFA-TAG eluted first, which were those having FA chains the same or similar lengths, such as LaLaLa (three C12:0 FA lengths) in Fig. 7D. Then, the next more heterogeneous eluted, with a greater disparity between FA chain lengths, such as LaCaM (from C10:0 to C14:0 FA lengths) in Fig. 7E. Then, the most heterogeneous isomer eluted, with the greatest disparity between FA chains, such as LaCyP (from C8:0 to C16:0 FA lengths) in Fig. 7F. This pattern is typical behavior based on the longest chain being the dominant factor in retention on a C18 column with non-aqueous reversed phase solvents (ACN/DCM). If this pattern is continued, the next isomer would have C6:0 to C18:0 FA lengths, meaning that LaCoS would elute next. Indeed, the mass spectrum across the small peak at 26.59 min in Fig. 7C does show [LaCo]<sup>+</sup> at *m/z* 355.3 and [LaS]<sup>+</sup> at *m/z* 523.5, as expected, though the peaks are chromatographically overlapped by a more abundant TAG molecular species and its fragments (LLLn, data not shown).

Thus, the [M+NH<sub>4</sub>]<sup>+</sup> adducts, combined with the [DAG]<sup>+</sup> fragments allowed facile qualitative identification of TAGs and TAG isomers within peaks. While extremely valuable for qualitative identification, the presence of [DAG]<sup>+</sup> fragments in mass spectra such as shown in Fig. 7 render these ESI-MS data unusable for lipidomics based on LipidSearch software. Since running these experiments, the instrument has been re-tuned and calibrated such that all ions except [M+NH<sub>4</sub>]<sup>+</sup> ions were minimized, to allow lipidomic software analysis, at the expense of easy visual analysis using [DAG]<sup>+</sup>.

### 3.4. Triacylglycerols in the <sup>2</sup>D(1)

Conventional 2D-LC approaches demand elution of all of a sample bolus from one modulation period before the beginning of the next modulation period. This is often accomplished using a combination of high <sup>2</sup>D flow rates with sharp solvent gradients to quickly elute analytes from the <sup>2</sup>D before the next bolus is injected by the 2D valve. Such high flow rates also help dilute incompatible solvents. However, our experimental arrangement is different.

We use a split flow approach, and our <sup>2</sup>D(2) column was not orthogonal, but was incrementally more non-polar (C30 vs. C18). We tried shifted gradients on these columns, in which the sub-gradients were the length of the modulation period, similar to what we have reported previously [25]. We found no benefit to shifted gradients versus simple parallel gradient elution under these conditions, and the parallel gradient greatly simplified <sup>2</sup>D(2) solvent programming.

The MS cube/3D plot and mass spectrum in Fig. 8 show that SCFA-TAGs were better separated from MLCFA-TAGs than they were in the <sup>1</sup>D. A contour plot with these data is given in Supplementary Figure 7. The SCFA-TAGs clearly form an arc that eluted earlier and better separated from the MLCFA-TAGs than in the <sup>1</sup>D. Thus, the separation between SCFA and MLCFA was improved in <sup>2</sup>D(1), but the separation within categories, SCFA vs. MLCFA, was poorer in the <sup>2</sup>D(1). The ESI-MS mass spectrum obtained on the LCQ Deca XP ion trap mass spectrometer, Fig. 8C, employed 15 V of up-front collision-induced dissociation (UF-CID) energy applied to produce some [DAG]<sup>+</sup> fragments. It is much easier to identify TAGs using the 2D-LC imaging software if some UF-CID is applied and [DAG]<sup>+</sup> are visible in the full-scan spectrum, since accessing the MS/MS data in the 2D-LC software is not readily straightforward. The SCFA-TAGs exhibited more [M+Na]<sup>+</sup> adduct than we usually observe with other saturated FAs. This seemed to correlate with a higher amount of methanol in the mobile phase. In many cases the [M+Na]<sup>+</sup> adduct of SCFA-TAGs was the base peak.

Unfortunately, most SCFA-TAG peaks in Fig. 8 are still mixtures of SCFA-TAG isomers, so the SCFA-TAGs were not sufficiently separated using single-modulation period elution in the <sup>2</sup>D. Nevertheless, using <sup>2</sup>D(1) to elute the analytes in one modulation period was done to partially to satisfy the 2D-LC “purists” who want to

see analytes eluted in one modulation period. While useful information was obtained, the data pointed to the need for further separation.

### 3.5. Triacylglycerols in the <sup>2</sup>D(2)

Our most powerful HRAM-MS instrument was connected to the outlet of the <sup>2</sup>D(2), to take advantage of the best separation available on our system. LipidSearch lipidomics was used for detection of the <sup>2</sup>D(2), to avoid manual integration of peaks. Although we accomplished identification and semi-quantification (percent relative quantification) using LipidSearch, we recommend that others do not use it for <sup>2</sup>D detection. Having some peaks split into two modulation periods complicated the identification and quantification of TAGs. Areas from one or two modulation periods were summed to represent the total area of each identified TAG. We observed many idiosyncrasies of LipidSearch that indicate that it should be used carefully and with understanding of its shortcomings, even when used with 1D-LC or infusion.

*LipidSearch 4.2 software.* We allowed ThermoScientific LipidSearch (ver. 4.2) lipidomics software to perform identification and integration of peaks, but not alignment across all files. Conventional automated processing using LipidSearch led to many errors or shortcomings. Among these was loss of individual peak area data, with aligned peaks reporting only the average areas across all runs. Also, when peaks were aligned, all except four (4) digits were discarded and replaced with 0, giving all areas to only four significant figures. Furthermore, the exact integration times for every peak in each run were needed (to allow us to calculate the Critical Ratios [55,56], CRs, from the same mass spectrum), and those data were lost if all runs were aligned together. To overcome these shortcomings, files were aligned individually with themselves to maintain individual peak areas, retention times, and integration window parameters. Alignment of peaks (matching peaks from run to run) was done manually by identity and retention time in an Excel workbook. By analyzing all runs individually, percentage compositions for each run could be calculated with higher precision, and then averages obtained. Three samples, each with three replicates were used, so individual sample averages are given in Supplementary Table S-16, while the overall average is given in Table 3.

Next, there were peaks that could clearly manually be identified in the <sup>1</sup>D that the software did not identify in the <sup>2</sup>D(2). For instance, OOB and OOLg are clearly visible in the TIC in Fig. 7A, but they do not appear in Table 3. They were not identified by LipidSearch. But these results must be compared to the manual method we used to use. In that approach, we set up a processing method to integrate specified peaks. Those results were always based on multiple mutual confirmatory EICs, so we had good confidence in the identities assigned. There were always TAG peaks, usually minor, that could be qualitatively identified but which were not quantified. If a peak was found at a sufficient level it was added to the processing method. The major disadvantage was that all peaks were integrated manually, and a minor disadvantage was that unexpected and minor peaks were/may not be included.

Some TAGs were mis-identified, such as PLaP, which was not identified, but isomers present at lower levels (SMLa, LaLaA) were identified. TAGs that were thus mis-identified had to be manually identified using Xcalibur, and the composition calculated from the [DAG]<sup>+</sup> abundances from the mass spectrum of the overlapped isomers, with apportionment of overlapped [DAG]<sup>+</sup>. In cases of overlap of multiple isomers, statistically predicted ratios of [DAG]<sup>+</sup> fragments were used to apportion [DAG]<sup>+</sup> peaks, which gave better results than using idealized theoretical fragment ratios. Because of the apportionment of overlapped peaks, regioisomeric assignments

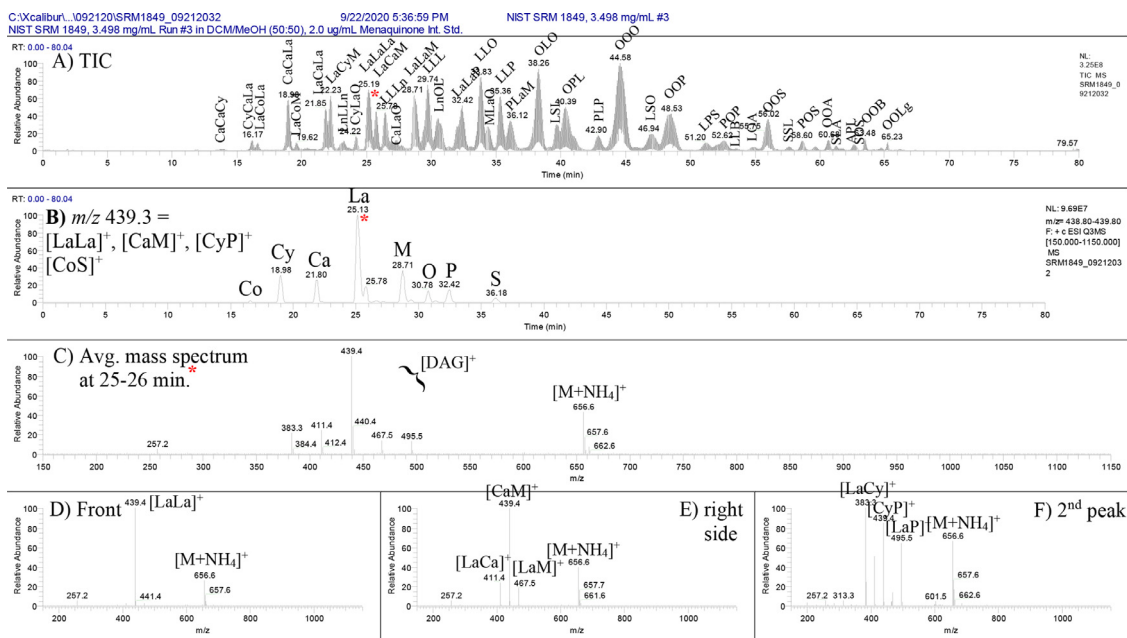


**Fig. 7.** A) Total ion current chromatogram (TIC). B) Extracted ion chromatogram (EIC) of  $m/z$  439.3 =  $[LaLa]^+$  =  $[CaM]^+$  =  $[CyP]^+$ . C) Average ESI-MS mass spectrum across peak at 24.70–26.04 min in B), indicating LaLaLa. D) Average mass spectrum at 24.70–25.07 min, at the front part of the largest peak in B), indicating LaCaM. E) Average mass spectrum at 25.07–25.45 min. F) Average mass spectrum at 25.45–25.94 min, indicating LaCyP.

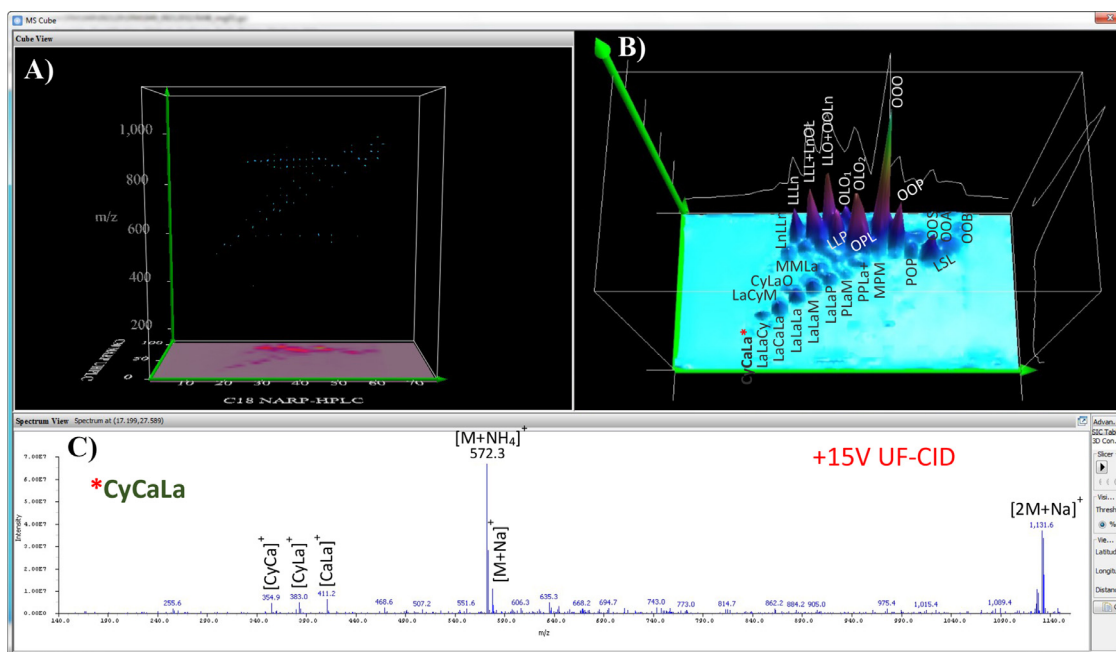


**Fig. 8.** MS cube/3D view of  $^2D(1)$  ESI-MS data from LCQ Deca XP mass spectrometer. Separation on  $50 \times 2.1$  mm,  $2.9 \mu m$  column at  $10^\circ C$  with solvent gradient ACN/DCM  $100/0\% \rightarrow 67/33\%$ . A) MS Cube view; B) 3D view; C) mass spectrum of CaCyLa, marked with red asterisk in B).

could not be made with as much confidence as they would be if peaks were all thoroughly resolved.

The main strength of LipidSearch was its ability to find and integrate peaks at low levels, that we would have ignored in the past. But the identification of those integrated peaks had to be checked carefully, and could not be considered reliable. Nevertheless, the peak integration was very helpful. So, there appears to be a tradeoff between accuracy and ease of integration. The LipidSearch software solves the problem of manual integration, but the results must be meticulously verified.

*Chromatography in the  $^2D(2)$ .* Fig. 9 shows the  $^2D(2)$  contour plot chromatogram from separation on the  $2 \times 25$  cm C18 columns plus the 100 mm C30 column, detected using the QExactive mass spectrometer with ESI-HRAM-MS. The parallel gradient used is in Fig. 3C. We used flow rate programming (FRP), Fig. 3C green line, to minimize and greatly reduce the overlap of wrapped-around TAGs with the modulation period top and bottom edges. We had even better runs from a preliminary sample set [57], that demonstrated that, with FRP, overlap can be almost eliminated. Those were preliminary data prior to quantification and regioisomer assignment, so the labels in that Fig. 5 [57] are not regioisomer specific.

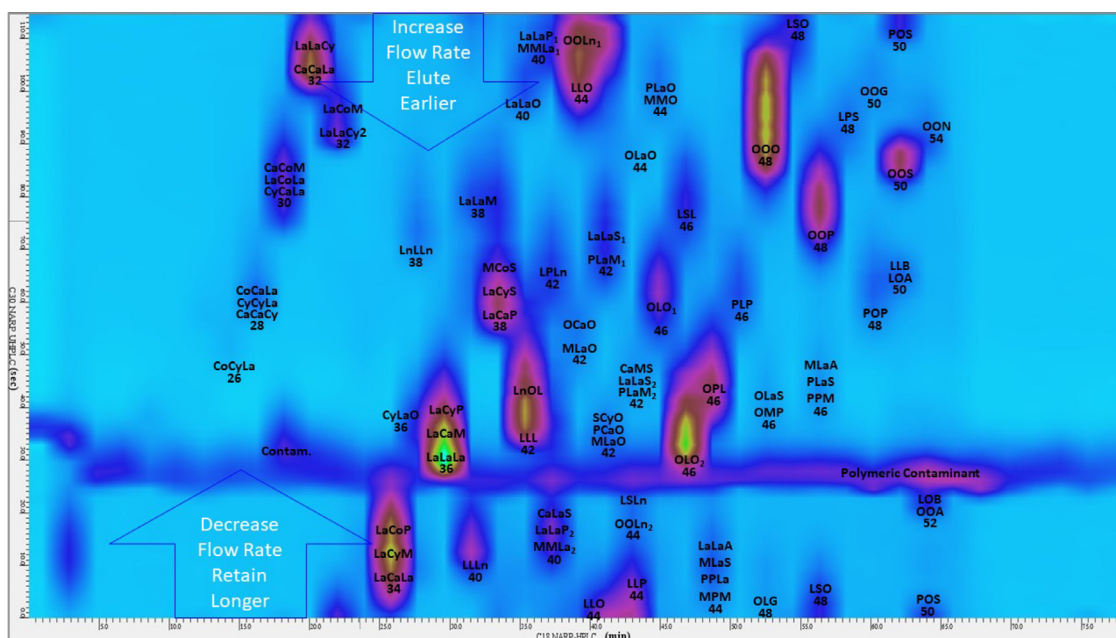


**Fig. 9.** Second second dimension,  $^2D(2)$ , contour plot chromatogram of NIST SRM 1849a using ESI-HRAM-MS detection. Flow rate programming was used to minimize border overlap using “controlled wraparound”. Short-chain fatty acid containing TAGs were still not completely resolved, but allowed partitioning of structural isomers.

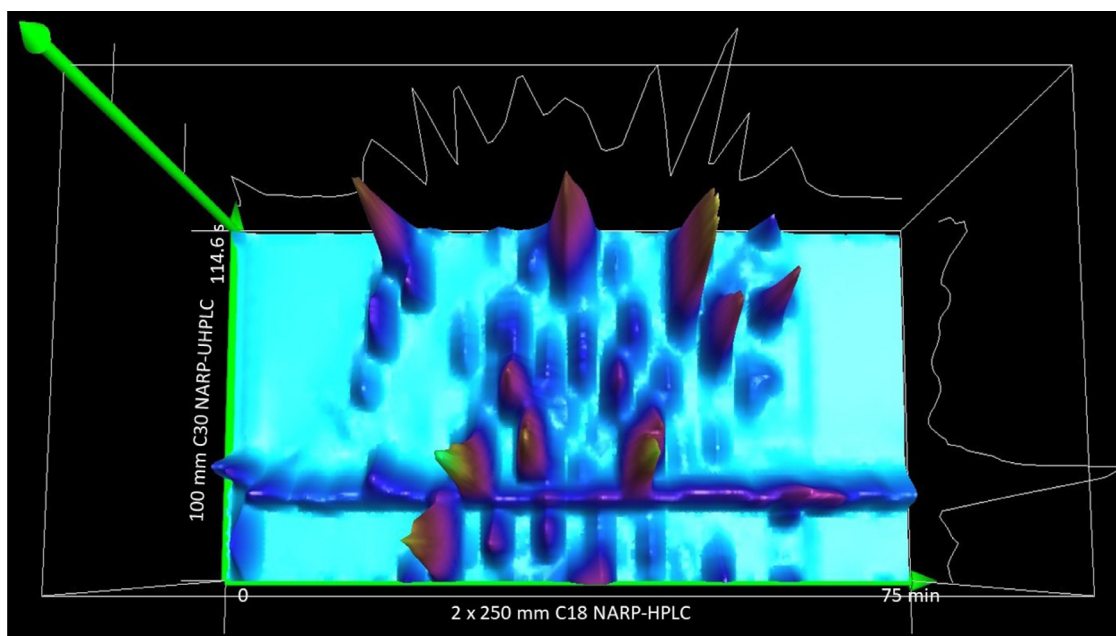


**Fig. 10.** Second second dimension,  $^2D(2)$ , 3-D plot chromatogram of NIST SRM 1849a using ESI-HRAM-MS detection. Single structural isomer peaks remained sharp after multiple modulation cycles, while mixtures of structural isomers (e.g., 10,10,10; 8,10,12; 6,10,14) partitioned across broadened peaks, with the most homogeneous TAG eluted first, then TAGs with moderate FA differences, followed by TAGs with the most heterogeneous FA.

Nevertheless, Fig. 9 nicely demonstrates the improved separation and partitioning of TAGs, compared to the  $^1D$ . Not only are more separated peaks visible, but peaks containing multiple isomers are elongated, as the isomers partially separated and partitioned across the peaks. Some peaks, such as OON, that are not isomer peaks, demonstrated how sharp and well-resolved the multi-cycle peaks could remain, with the use of TED solvent. Fig. 10 shows the 3-D plot chromatogram, giving a better view of peak shapes. Again, single TAG peaks such as OON (upper right in Fig. 10) gave very nice peak shapes with the use of TED solvent, despite being on the column through more than one modulation period. Based on the partial separations in partitioned peaks, it may be possible to

further improve the separation by allowing more time on column, through more modulation cycles, especially early in the run.

Some peaks that occurred at the time of a valve switch were split into two peaks differing by less than a full modulation period (1.91 min), such as MMLa + LaLaP, which gave a minor and a major peak in Fig. 9 differing by 1.55 min. A likely contributing factor was that a peak that was split by a valve switch had part of the peak in the tail end of the sample loop in the first modulation period, and the front of the sample loop in the next modulation period. Although the TED solvent kept the peaks fairly sharp, it did not cause TAGs to completely hold up at the front of the  $^2D$  column, as was the case in the orthogonal  $Ag^+$  ion chromatography [25]. So

the difference in positions in the sample loop could lead to differences in retention times in the  $^2D(2)$  (i.e., peak eluted late in the preceding modulation period and earlier in the succeeding modulation period). Also, the increasing solvent strength of the parallel gradient likely contributed to eluting TAGs in the second modulation period earlier than in the preceding modulation period.

**Regioisomer assignments.** The  $^2D(2)$  peaks were integrated by LipidSearch, and the beginning and ending times of integration were pasted into Xcalibur Qual Browser, and the spectrum list was obtained and copied to a spreadsheet for CR calculations. Peaks in

$$\%ABA = \left( \frac{([AA]^+ / [AB]^+)_{AAB} - ([AA]^+ / [AB]^+)_{obs}}{([AA]^+ / [AB]^+)_{AAB} - ([AA]^+ / [AB]^+)_{ABA}} \right) \quad (1)$$

Or, conversely, we can calculate:

$$\%AAB/BAA = \left( \frac{([AA]^+ / [AB]^+)_{obs} - ([AA]^+ / [AB]^+)_{ABA}}{([AA]^+ / [AB]^+)_{AAB} - ([AA]^+ / [AB]^+)_{ABA}} \right) \quad (2)$$

some runs eluted during a valve switch, and so appeared in more than one modulation period. The number of runs in which a peak was observed, if not all, is indicated in brackets in Table 3. Some had isomers that went into a third modulation period.

Regioisomers of Type III TAGs [56] like LaCaM and LaCyP were assigned their specific structures by reference to precedent [28,55,56,58,59] that indicates loss of the FA in the *sn*-2 position is disfavored, so the smallest [DAG]<sup>+</sup> ion in spectra of ABC TAGs is the [1,3-AC]<sup>+</sup> fragment. For instance, even though Fig. 7E shows a  $^1D$  spectrum, we can see use it as an example of a spectrum with [LaM]<sup>+</sup> as the smallest [DAG]<sup>+</sup> fragment, indicating it is the [1,3-LaM]<sup>+</sup> fragment. We cannot determine with further specificity whether it is the [*sn*1,3-LaM]<sup>+</sup> or [*sn*1,3-MLa]<sup>+</sup>, since these come from stereoisomers LaCaM and MLaLa, that would require very lengthy chiral chromatography to fully resolve [60,61]. Thus, we chose to apply the Byrdwell convention [55,56] for Critical Ratio 3, the [BC]<sup>+</sup>/[AB]<sup>+</sup> ratio, which is to select the name assignment based on [BC]<sup>+</sup>/[AB]<sup>+</sup> that gives CR3 < 1. By applying the Byrdwell convention for CR3, we can observe if there are any trends in which FA end up in the numerator versus the denominator. We previously used CR3 to show that for normal TAGs with some PUFA, the [DAG]<sup>+</sup> fragment with more unsaturation was the larger fragment, in most cases [56].

Regioisomers of Type II TAGs, ABA/AAB/BAA, were qualitatively and quantitatively specified to the greatest extent possible in Table 3, using theoretical principles, published values [59], and laboratory empirical values for Critical Ratio 2, CR2, the [AA]<sup>+</sup>/[AB]<sup>+</sup> ratio. We have recently added some regioisomer quantitative standards to our calibration mixture, to be reported soon, and have used ratios from the new calibration standards for relative regioisomer quantification for 10 molecular species.

Theoretically, if there were no non-statistical influences, the ratio of [AA]<sup>+</sup>/[AB]<sup>+</sup> should always be 1/2 or 0.5 for all isomers, which corresponds to the Critical Value for Type II TAGs [56]. Therefore, as the first crude approximation, CR2 < 0.5 tends to indicate less [AA]<sup>+</sup> and so more ABA isomer, while a CR2 > 0.5 tends to indicate more [AA]<sup>+</sup> and less ABA isomer. Of course, carbon chain length and degree of unsaturation have the effects referenced above, so the value of 0.5 is only the first indicator, and not reliable by itself for assignment with confidence.

Comparison to literature values [59] was valuable. However, those values were from APCI-MS. We used the same brand and model of instrument as one described [59], but we employed ESI-MS instead of APCI-MS. Nevertheless, we have previously shown that the agreement between ESI-MS and APCI-MS is good, but not quite as good as the agreement between APPI-MS and APCI-MS

[55]. Table 2 in that report [59] does confirm the principle above, since every 100% ABA TAG had a CR2 < 0.5, while every 100% AAB/BAA TAG had a CR2 > 0.5.

An example of regioisomer composition estimation using literature values is seen in LLLn in Supplementary Table S-17. The Type II TAG LLLn/LLn/LnLL gave a CR2 of 0.61 in Table S-17. Literature values ranged from 0.38 (±0.04) to 0.68 (±0.06). The fact that our CR2 > 0.5, and the fact that it is close to the upper value for 100% AAB/BAA (0% ABA), already provide strong indications that the TAG is mostly LLLn/LnLL. Using the equations first reported by Byrdwell [53], derived from the work of Jakab, et al. [62], we can calculate:

Using Eq. (2), we calculate that a CR2 of 0.61 gives: %AAB/BAA = ((0.61-0.38) / (0.68-0.38)) = 76.7% LLLn/LnLL. The values in Table S-17 were calculated using un-rounded CR2 values, not to 2 decimal places, so they are more precise than these examples. Thus these calculations indicate that the Type II TAG LLLn/LLn/LnLL was ~3/4 LLLn/LnLL and ~1/4 LLLn. Still, any calculation based on literature values should be considered an estimation.

For some TAGs, such as LLLn in Supplementary Table S-17, which has a CR2 = 0.39, their CR2 was outside the range of the literature values. This was itself strongly indicative of structure. For example, the literature values from Holcapek [59] indicated that LLLn/LLn/LnLL gave CR2 values from 0.46 to 0.75. It was low, at 0.46, for the pure ABA isomer LLLn. Notice that this is barely lower than the statistically theoretical value of 0.5. CR2 was high for the AAB/BAA isomers, LLLn/LLn/LnLL, well above the statistically predicted value of 0.5. Thus, when our value of 0.39 is even lower than the literature value for LLLn, we can have good confidence that the Type II TAG in the NIST SRM 1849a is in the form of the ABA isomer LLLn. Similarly, a Type II TAG with CR2 above the range of a 100% AAB/BAA TAG, such as LLP in Table S-17, is a strong indicator of the likely identity as the AAB/BAA regioisomer pair, in this case LLP/PLL.

Ten regioisomers were quantified using regioisomeric standards analyzed in our lab. For example, LaLaM in Table S-17, which gave a CR2 of 0.64. First, the fact that CR2 > 0.5 indicates that it is likely AAB/BAA. The regioisomer standards LaMLa and LaLaM gave CR2 values of 0.38 and 0.66 for the 100% ABA isomer and 100% AAB/BAA isomers, respectively. From Eq. (2), CR2<sub>obs</sub> = 0.64 gives an estimate of 93% of the LaLaM/MLaLa isomers. Despite this being calculated from empirical results, the complete set of regioisomer calibration standards with replicates has not yet been reported, so these values should be considered estimates until additional data from multiple replicates at multiple concentrations are reported with statistical treatment.

By the combination of whether the CR2 < 0.5 or CR2 > 0.5, literature values, and empirical laboratory values, we were able to make regioisomeric assignments for all (including Type I TAGs) except 9 TAGs and estimate the compositions of 20 Type II TAG regioisomers, 10 using literature values, and 10 TAGs estimated using regioisomer standards.

**TAG% Composition adjusted to GC-FID.** The SCFA-TAG isomers were better separated in the  $^2D(2)$  than they were in the  $^1D$ , but they were still only partially separated, or partitioned, within the  $^2D(2)$  peaks. As discussed regarding the  $^1D$  data, sequentially viewing mass spectra in a peak, or "stepping across" the peaks revealed that the most homogeneous SCFA-TAG eluted first, then the next more heterogeneous eluted, with a greater disparity between FA

chain lengths, such as LaCaM in Fig. 7E and Fig. S-5E. Then, the most heterogeneous isomer eluted, with the greatest disparity between FA chains, such as CyLaP in Fig. S-5F. But for quantification purposes, the  $[M+NH_4]^+$  peak areas had to be integrated together, and the peak areas apportioned into different TAGs based on the  $[DAG]^+$  fragments in the mass spectra across the peak.

The average compositions of TAGs from individual treatment of files in LipidSearch are given in Table 3. The raw TAG% is prior to application of any response factors (RFs), and so is of limited use other than to demonstrate the direction of over-response or under-response. One can see by comparison of the TIC by APCI-MS, Fig. 5A, to the TIC by ESI-MS, Fig. 7A, that the TAGs respond differently to ESI versus APCI and require RFs. The GC-FID RF adjusted TAG% is the best estimate of the NIST SRM TAG% composition based on our LC-MS and GC-FID results. Comparison of response-factor adjusted results ("GC-FID RF Adj. TAG%") to raw results ("Raw TAG%") reveals the overall trend in TAG response. The SCFA TAG eluted earlier, are higher in the table (sorted by retention time, RT), and tended to have RF-adjusted results lower than raw results (raw percentages are being brought down), meaning they over-responded in raw LC-MS results. Early eluting PUFA TAG such as LnLLn also over-responded and were brought down in RF-adjusted results. It is well known that PUFA TAGs respond better to ESI-MS [28]. Conversely, as the carbon chain length increased and the degree of unsaturation decreased, retention time increased, and the values lower in Table 3 (later RT) had raw values that were often lower than RF-adjusted values, especially for TAGs with oleic acid, O, indicating these under-responded and were being adjusted upward.

One slight trend that seemed to be evident was that it was commonly, but not always, observed that the shortest FA preferred the 2-position, such that the shortest of three FAs was often in the 2-position of the TAGs, and if there were two short and one longer FA, the longer FA was in a 1,3-position. Sixty-five (65) out of 85 TAGs containing SCFA had the shortest FA in the 2-position of Type III TAGs or a short FA in the 2-position of Type II TAGs, constituting ~76% of SCFA TAGs.

TAG% Composition adjusted to the NIST SRM COA. Table 3 also includes the TAG composition adjusted to the consensus GC-FID target values in the SRM COA. Since the certificate values are also from GC-FID data of the same material, it is appropriate to adjust the raw TAG% results to those best estimate true values to get the best estimate true TAG composition, and compare it to the TAG composition adjusted to our laboratory GC-FID values.

The differences between the true-value-adjusted TAG% and our GC-FID adjusted TAG% are small, as seen in the last column in Table 3. The largest difference between any two values is 0.47% difference between 13.67% ( $\pm 0.47$ ) by GC-FID and 13.20% ( $\pm 0.46$ ) by COA. Although the difference is more than the uncertainty in either individual value, it is well within the overlapping ranges of uncertainties and is less than the square root of the sum of the squares of the two values ( $= 0.66\%$ ), meaning the difference is not statistically significant. Many of the differences are so small that they are within the uncertainty of the individual values, meaning they are indistinguishable within the run-to-run variability. Only a few TAGs had differences that were greater than the uncertainty in values, and those case were mostly because the run-to-run variability was so low. Thus, we can say that there is good agreement between the TAG% composition adjusted to the NIST SRM COA and adjusted to our GC-FID results. And we can say that the GC-FID adjusted TAG% composition is a very good approximation of the TAG% composition based on the best estimate for the true FA composition. Furthermore, we can extrapolate from these results to say that even when an SRM for FA% composition is not available, the GC-FID adjusted TAG% composition gives a good estimate of the

composition of a TAG mixture, as long as the criteria for the FA RF approach, mentioned above, are met.

#### 4. Conclusion

We have reported here experiments that provided three dimensions of chromatographic separation coupled with four mass spectrometers, LC3MS4, using split-flow comprehensive multidimensional liquid chromatography (SF-CMDLC) having two parallel second dimensions, LC1MS2 (LC1MS1 + LC1MS1). The second second dimension, 2D(2), UHPLC was connected to two contact closure controlled valves controlled by a timed contact closure circuit (TCCC) via a wireless communication contact closure system (WC-CCS). The multiple first reports, innovations, and accomplishments in this report are best summarized as follows:

- First report of split-flow comprehensive three-dimensional liquid chromatography, SF-C3DLC, with parallel  $^2D$ s and four mass spectrometers, LC3MS4.
- Demonstrated quantification of FSVs by EICs, SIM, and SRM in the  $^1D$  of SF-C3DLC.
- Obtained very good to excellent agreement between our value and NIST SRM certificate of analysis (COA) values for retinyl palmitate and  $\alpha$ -tocopheryl acetate.
- Obtained very good agreement in our values for FA mole% composition vs. NIST SRM COA.
- Demonstration of the use of transferred eluent dilution (TED) solvent to minimize peak broadening in SF-C3DLC.
- Demonstrated the use of "constructive wraparound" or multi-cycle SF-C3DLC.
- Demonstrated the use of flow rate programming (FRP) in the  $^2D(2)$  to better control the overlap of multi-cycle peaks, for FRP-controlled multi-cycle LC.
- Demonstrated the first use of lipidomics software in the  $^2D(2)$  to produce a GC-FID adjusted TAG% composition.
- Only 9 TAGs had undefined regioisomers, accounting for 93.8% of TAGs assigned (including Type I TAGs).
- Identified trend that in ~76% of SCFA TAGs, the shortest FA was in the 2-position.
- Estimated regioisomeric compositions of 10 TAGs based on literature values for Critical Ratio 2 (CR2).
- Estimated regioisomeric composition of 10 TAGs based on empirical lab values for CR2.

Finally, we have provided a table of the CRs in the Supplementary Table S-17, because the CRs constitute a compressed library of mass spectra, since the mass spectra can be reproduced by processing the CRs through the UBUS [55,63].

These data have provided valuable insights into the structures of the different pools of TAGs in the formulated NIST SRM 1849a. These experiments also pointed toward improvements and modifications that can be made to the experimental arrangement. The ESI-HRAM-MS instrument has been reconnected to the HPLC for lipidomic analysis in the  $^1D$ . We have already conducted preliminary experiments combining the best aspects of LC2MS4 [25] and these LC3MS4 experiments, to allow 2 x C18 in the  $^1D$ , Ag<sup>+</sup> in the  $^2D(1)$ , and multi-cycle C30 in the  $^2D(2)$ . As mentioned, we have improved the calibration standard set to include TAGs and TAG regioisomers, to be reported soon.

#### Authors' contribution

William Byrdwell (conception and design of the study, acquisition of data, analysis and/or interpretation of data, drafting the manuscript, revising the manuscript, submitting the manuscript); Hari Kotapati (data analysis and/or interpretation of data, drafting the manuscript); Robert Goldschmidt (acquisition of data, analysis

and/or interpretation of data); Pavel Jakubec (conception and design of the study); Lucie Novakova (conception and design of the study, financial support of Pavel Jakubec).

### Declaration of Competing Interest

The authors declare that they have no known competing financial interests or personal relationships that could have appeared to influence the work reported in this paper.

### Acknowledgment

This work was supported by the [USDA Agricultural Research Service](#). Mention or use of specific products or brands do not represent or imply endorsement by the USDA. Pavel Jakubec worked in the Byrdwell laboratory through a collaboration with Prof. Lucie Nováková, funded by fellowship # CZ.02.1.01/0.0/0.0/15\_003/0000465, Specialized Team for Advanced Research on Separation Science (STARSS), provided by The [European Social Fund \(ESF\)](#) and the [European Regional Development Fund \(ERDF\)](#), Operational Programme Research, Development and Education PO1.SC1.IP1.

### Supplementary materials

Supplementary material associated with this article can be found, in the online version, at doi:[10.1016/j.chroma.2021.462682](https://doi.org/10.1016/j.chroma.2021.462682).

### References

- J.C. Giddings, Two-dimensional separations: concept and promise, *Anal. Chem.* 56 (1984) 1258A–1264A, doi:[10.1021/ac00276a003](https://doi.org/10.1021/ac00276a003).
- D.R. Stoll, X. Li, X. Wang, P.W. Carr, S.E.G. Porter, S.C. Rutan, Fast, comprehensive two-dimensional liquid chromatography, *J. Chromatogr. A* 1168 (2007) 3–43, doi:[10.1016/j.chroma.2007.08.054](https://doi.org/10.1016/j.chroma.2007.08.054).
- D.R. Stoll, P.W. Carr, Two-Dimensional Liquid Chromatography: a State of the Art Tutorial, *Anal. Chem.* 89 (2017) 519–531, doi:[10.1021/acs.analchem.6b03506](https://doi.org/10.1021/acs.analchem.6b03506).
- Z. Wu, P. Schoenmakers, P.J. Marriott, Nomenclature and Conventions in Comprehensive Multidimensional Chromatography - An Update, *LCGC Eur* 25 (2012) 272–275.
- B.W.J. Pirok, A.F.G. Gargano, P.J. Schoenmakers, Optimizing separations in on-line comprehensive two-dimensional liquid chromatography, *J. Sep. Sci.* 41 (2018) 68–98, doi:[10.1002/jssc.201700863](https://doi.org/10.1002/jssc.201700863).
- B.W.J. Pirok, P.J. Schoenmakers, Practical approaches to overcome the challenges of comprehensive two-dimensional liquid chromatography, *LC-GC Eur* 31 (2018) 242–249.
- D.R. Stoll, K. Shoykhet, P. Petersson, S. Buckenmaier, Active Solvent Modulation: a Valve-Based Approach to Improve Separation Compatibility in Two-Dimensional Liquid Chromatography, *Anal. Chem.* 89 (2017) 9260–9267, doi:[10.1021/acs.analchem.7b02046](https://doi.org/10.1021/acs.analchem.7b02046).
- J.V. Seeley, F.J. Kramp, K.S. Sharpe, A dual-secondary column comprehensive two-dimensional gas chromatograph for the analysis of volatile organic compound mixtures, *J. Sep. Sci.* 24 (2001) 444–450, doi:[10.1002/1615-9314\(20010601\)24:6\(444\)::AID--JSSC444>3.0.CO;2-5](https://doi.org/10.1002/1615-9314(20010601)24:6(444)::AID--JSSC444>3.0.CO;2-5).
- J.V. Seeley, F.J. Kramp, K.S. Sharpe, S.K. Seeley, Characterization of gaseous mixtures of organic compounds with dual-secondary column comprehensive two-dimensional gas chromatography (GC × 2 GC), *J. Sep. Sci.* 25 (2002) 53–59, doi:[10.1002/1615-9314\(20020101\)25:1/2\(53\)::AID--JSSC53>3.0.CO;2-V](https://doi.org/10.1002/1615-9314(20020101)25:1/2(53)::AID--JSSC53>3.0.CO;2-V).
- B. Savareear, R.A. Shellie, Multiplexed dual second-dimension column comprehensive two-dimensional gas chromatography (GC×2GC) using thermal modulation and contra-directional second-dimension columns, *Anal. Chim. Acta.* 803 (2013) 160–165, doi:[10.1016/j.aca.2013.05.013](https://doi.org/10.1016/j.aca.2013.05.013).
- S.E. Reichenbach, D.W. Remppe, Q. Tao, D. Bressanello, E. Libertò, C. Bicchi, S. Balducci, C. Cordero, Alignment for Comprehensive Two-Dimensional Gas Chromatography with Dual Secondary Columns and Detectors, *Anal. Chem.* 87 (2015) 10056–10063, doi:[10.1021/acs.analchem.5b02718](https://doi.org/10.1021/acs.analchem.5b02718).
- B. Sgorbini, C. Cagliero, L. Boggia, E. Libertò, S.E. Reichenbach, P. Rubiolo, C. Cordero, C. Bicchi, Parallel dual secondary-column-dual detection comprehensive two-dimensional gas chromatography: a flexible and reliable analytical tool for essential oils quantitative profiling, *Flavour Fragr. J.* 30 (2015) 366–380, doi:[10.1002/ffj.3255](https://doi.org/10.1002/ffj.3255).
- B. Savareear, M.R. Jacobs, R.A. Shellie, Multiplexed dual first-dimension comprehensive two-dimensional gas chromatography-mass spectrometry with contra-directional thermal modulation, *J. Chromatogr. A* 1365 (2014) 183–190, doi:[10.1016/j.chroma.2014.09.014](https://doi.org/10.1016/j.chroma.2014.09.014).
- D. Yan, L. Tedone, A. Koutoulis, S.P. Whittock, R.A. Shellie, Parallel comprehensive two-dimensional gas chromatography, *J. Chromatogr. A* 1524 (2017) 202–209, doi:[10.1016/j.chroma.2017.09.063](https://doi.org/10.1016/j.chroma.2017.09.063).
- A.J. Link, J. Eng, D.M. Schieltz, E. Carmack, G.J. Mize, D.R. Morris, B.M. Garvik, J.R. Yates III, Direct analysis of protein complexes using mass spectrometry, *Nat. Biotechnol.* 17 (1999) 676–682, doi:[10.1038/10890](https://doi.org/10.1038/10890).
- M.P. Washburn, D. Wolters, J.R. Yates, Large-scale analysis of the yeast proteome by multidimensional protein identification technology, *Nat. Biotechnol.* 19 (2001) 242–247, doi:[10.1038/85686](https://doi.org/10.1038/85686).
- V.-A. Duong, J.-M. Park, H. Lee, Review of three-dimensional liquid chromatography platforms for bottom-up proteomics, *Int. J. Mol. Sci.* 21 (2020), doi:[10.3390/ijms21041524](https://doi.org/10.3390/ijms21041524).
- K. Feng, S. Wang, L. Han, Y. Qian, H. Li, X. Li, L. Jia, Y. Hu, H. Wang, M. Liu, W. Hu, D. Guo, W. Yang, Configuration of the ion exchange chromatography, hydrophilic interaction chromatography, and reversed-phase chromatography as off-line three-dimensional chromatography coupled with high-resolution quadrupole-Orbitrap mass spectrometry for the multicomponent, *J. Chromatogr. A* (2021) 1649, doi:[10.1016/j.chroma.2021.462237](https://doi.org/10.1016/j.chroma.2021.462237).
- J. Wei, J. Sun, W. Yu, A. Jones, P. Oeller, M. Keller, G. Woodnutt, J.M. Short, Global proteome discovery using an online three-dimensional LC-MS/MS, *J. Proteome Res.* 4 (2005) 801–808, doi:[10.1021/pr0497632](https://doi.org/10.1021/pr0497632).
- S. Wang, X. Shi, G. Xu, Online Three Dimensional Liquid Chromatography/Mass Spectrometry Method for the Separation of Complex Samples, *Anal. Chem.* 89 (2017) 1433–1438, doi:[10.1021/acs.analchem.6b04401](https://doi.org/10.1021/acs.analchem.6b04401).
- J. Camperi, L. Dai, D. Guillaume, C. Stella, Development of a 3D-LC/MS Workflow for Fast, Automated, and Effective Characterization of Glycosylation Patterns of Biotherapeutic Products, *Anal. Chem.* 92 (2020) 4357–4363, doi:[10.1021/acs.analchem.9b05193](https://doi.org/10.1021/acs.analchem.9b05193).
- S.W. Simpkins, J.W. Bedard, S.R. Groskreutz, M.M. Swenson, T.E. Liskutin, D.R. Stoll, Targeted three-dimensional liquid chromatography: a versatile tool for quantitative trace analysis in complex matrices, *J. Chromatogr. A* 1217 (2010) 7648–7660, doi:[10.1016/j.chroma.2010.09.023](https://doi.org/10.1016/j.chroma.2010.09.023).
- Y. Oda, N. Asakawa, T. Kajima, Y. Yoshida, T. Sato, On-line determination and resolution of verapamil enantiomers by high-performance liquid chromatography with column switching, *J. Chromatogr. A* 541 (1991) 411–418, doi:[10.1016/S0021-9673\(01\)96013-3](https://doi.org/10.1016/S0021-9673(01)96013-3).
- A.W. Moore Jr., J.W. Jorgenson, Comprehensive Three-Dimensional Separation of Peptides Using Size Exclusion Chromatography/Reversed Phase Liquid Chromatography/Optically Gated Capillary Zone Electrophoresis, *Anal. Chem.* 67 (1995) 3456–3463, doi:[10.1021/ac00115a014](https://doi.org/10.1021/ac00115a014).
- W.C. Byrdwell, Comprehensive Dual Liquid Chromatography with Quadrupole Mass Spectrometry (LC1MS2 × LC1MS2 = LC2MS4) for Analysis of Parinari Curatellifolia and Other Seed Oil Triacylglycerols, *Anal. Chem.* 89 (2017) 10537–10546, doi:[10.1021/acs.analchem.7b02753](https://doi.org/10.1021/acs.analchem.7b02753).
- W.C. Byrdwell, Blue jacaranda seed oil analysed using comprehensive two dimensional liquid chromatography with quadrupole parallel mass spectrometry, *Chromatogr. Today* (2018) 56–64 May/June <https://www.chromatographytoday.com/article/lcxl/49/scientific-solutions/pblue-jacaranda-seed-oil-analysed-using-comprehensive-two-dimensional-liquid-chromatography-with-quadrupole-parallel-mass-spectrometry/2381>.
- W.C. Byrdwell, Dual parallel mass spectrometers for analysis of sphingolipid, glycerophospholipid and plasmalogen molecular species, *Rapid Commun. Mass Spectrom.* 12 (1998) 256–272, doi:[10.1002/\(SICI\)1097-0231\(19980314\)12:5\(256::AID--RCM149\)3.0.CO;2-8](https://doi.org/10.1002/(SICI)1097-0231(19980314)12:5(256::AID--RCM149)3.0.CO;2-8).
- W.C. Byrdwell, W.E. Neff, Dual parallel electrospray ionization and atmospheric pressure chemical ionization mass spectrometry (MS), MS/MS and MS/MS/MS for the analysis of triacylglycerols and triacylglycerol oxidation products, *Rapid Commun. Mass Spectrom.* 16 (2002) 300–319, doi:[10.1002/rcm.581](https://doi.org/10.1002/rcm.581).
- W.C. Byrdwell, Dual parallel liquid chromatography/mass spectrometry for lipid analysis, in: W.C. Byrdwell (Ed.), *Mod. Methods Lipid Anal. by Liq. Chromatogr. Mass Spectrom. Relat. Tech.*, Champaign, IL, AOCS Press, 2005, pp. 510–576.
- W.C. Byrdwell, Dual parallel liquid chromatography with dual mass spectrometry (LC2/MS2) for a total lipid analysis, *Front. Biosci.* 13 (2008) 100–120, doi:[10.2741/2663](https://doi.org/10.2741/2663).
- W.C. Byrdwell, Dual parallel mass spectrometry for lipid and vitamin D analysis, *J. Chromatogr. A* 1217 (2010) 3992–4003, doi:[10.1016/j.chroma.2009.11.101](https://doi.org/10.1016/j.chroma.2009.11.101).
- W.C. Byrdwell, Construction of a Wireless Communication Contact Closure System for Liquid Chromatography with Multiple Parallel Mass Spectrometers and Other Detectors, *J. Lab. Autom.* 19 (2014) 461–467, doi:[10.1177/2211068214543372](https://doi.org/10.1177/2211068214543372).
- W.C. Byrdwell, Timed relay contact closure controlled system for parallel second dimensions in multi-dimensional liquid chromatography, *BMC Res. Notes.* 12 (2019) 477, doi:[10.1186/s13104-019-4506-7](https://doi.org/10.1186/s13104-019-4506-7).
- Q. Liu, J. Xiao, J. Yu, Y. Xie, X. Chen, H. Yang, Improved enantioseparation via the twin-column based recycling high performance liquid chromatography, *J. Chromatogr. A* 1363 (2014) 236–241, doi:[10.1016/j.chroma.2014.07.040](https://doi.org/10.1016/j.chroma.2014.07.040).
- F. Gritti, S. Besner, S. Cormier, M. Gilar, Applications of high-resolution recycling liquid chromatography: from small to large molecules, *J. Chromatogr. A* 1524 (2017) 108–120, doi:[10.1016/j.chroma.2017.09.054](https://doi.org/10.1016/j.chroma.2017.09.054).
- F. Gritti, M. Leal, T. McDonald, M. Gilar, Ideal versus real automated twin column recycling chromatography process, *J. Chromatogr. A* 1508 (2017) 81–94, doi:[10.1016/j.chroma.2017.06.009](https://doi.org/10.1016/j.chroma.2017.06.009).
- F. Cacciola, P. Jandera, Z. Hajdú, P. Česla, L. Mondello, Comprehensive two-dimensional liquid chromatography with parallel gradients for separation of

- phenolic and flavone antioxidants, *J. Chromatogr. A.* 1149 (2007) 73–87, doi:10.1016/j.chroma.2007.01.119.
- [38] A.A. Aly, M. Muller, A. de Villiers, B.W.J. Pirok, T. Górecki, Parallel gradients in comprehensive multidimensional liquid chromatography enhance utilization of the separation space and the degree of orthogonality when the separation mechanisms are correlated, *J. Chromatogr. A.* 1628 (2020) 461452, doi:10.1016/j.chroma.2020.461452.
- [39] M. Russo, F. Cichello, C. Ragonese, P. Donato, F. Cacciola, P. Dugo, L. Mondello, Profiling and quantifying polar lipids in milk by hydrophilic interaction liquid chromatography coupled with evaporative light-scattering and mass spectrometry detection, *Anal. Bioanal. Chem.* 405 (2013) 4617–4626, doi:10.1007/s00216-012-6699-7.
- [40] J. Folch, M. Lees, G.H. Sloane-Stanley, A simple method for the isolation and purification of total lipides from animal tissue, *J. Biol. Chem.* 226 (1957) 497–509.
- [41] W.C. Byrdwell, “dilute-and-shoot” triple parallel mass spectrometry method for analysis of vitamin D and triacylglycerols in dietary supplements, *Anal. Bioanal. Chem.* 401 (2011) 3317–3334, doi:10.1007/s00216-011-5406-4.
- [42] W.C. Byrdwell, A note on the use of workstation software programs for quantification, *J. Liq. Chromatogr. Relat. Technol.* 42 (2019) 570–574, doi:10.1080/10826076.2019.1637350.
- [43] O. Podlaha, B. Töregård, A system for identification of triglycerides in reversed phase HPLC chromatograms based on equivalent carbon numbers, *J. High Resolut. Chromatogr.* 5 (1982) 553–558, doi:10.1002/jhrc.1240051007.
- [44] B. Herslöf, O. Podlaha, B. Töregård, HPLC of triglycerides, *J. Am. Oil Chem. Soc.* 56 (1979) 864–866, doi:10.1007/BF02909537.
- [45] C. Litchfield, Triglyceride analysis by consecutive liquid-liquid partition and gas-liquid chromatography. Ephedra nevadensis seed fat, *Lipids* 3 (1968) 170–177, doi:10.1007/BF02531736.
- [46] W.C. Byrdwell, Quadruple parallel mass spectrometry for analysis of vitamin D and triacylglycerols in a dietary supplement, *J. Chromatogr. A.* 1320 (2013) 48–65, doi:10.1016/j.chroma.2013.10.031.
- [47] C.A. Gonzalez, S.J. Choquette, Certificate of Analysis, Standard Reference Material 1849a, Natl. Inst. Stand. Technol. (2018) 1–13 <https://www-s.nist.gov/srmors/certificates/1849A.pdf>.
- [48] W.C. Byrdwell, E.A. Emken, W.E. Neff, R.O. Adlof, Quantitative analysis of triglycerides using atmospheric pressure chemical ionization-mass spectrometry, *Lipids* 31 (1996) 919–935, doi:10.1007/BF02522685.
- [49] W.C. Byrdwell, W.E. Neff, *Qualitative and Quantitative Analysis of Triacylglycerols Using Atmospheric Pressure Chemical Ionization Mass Spectrometry*, in: *New Tech. Appl. Lipid Anal.*, Champaign, IL, AOCS Press, 1997, pp. 45–80.
- [50] W.C. Byrdwell, W.E.W.E. Neff, G.R. List, W.Craig C. Byrdwell, W.E. Neff, G.R. List, Triacylglycerol analysis of potential margarine base stocks by high-performance liquid chromatography with atmospheric pressure chemical ionization mass spectrometry and, flame ionization detection, *J. Agric. Food Chem.* 49 (2001) 446–457, doi:10.1021/jf0008801.
- [51] X. Han, R.W. Gross, Quantitative analysis and molecular species fingerprinting of triacylglyceride molecular species directly from lipid extracts of biological samples by electrospray ionization tandem mass spectrometry, *Anal. Biochem.* 295 (2001) 88–100, doi:10.1006/abio.2001.5178.
- [52] W.E. Neff, G.R. List, W.C. Byrdwell, Effect of Triacylglycerol Composition on Functionality of Margarine Basestocks, *LWT - Food Sci. Technol.* 32 (1999) 416–424, doi:10.1006/food.1999.0571.
- [53] W.C. Byrdwell, *Qualitative and Quantitative Analysis of Triacylglycerols by Atmospheric Pressure Ionization (APCI and ESI) Mass Spectrometry Techniques*, in: W.C. Byrdwell (Ed.), *Mod. Methods Lipid Anal. by Liq. Chromatogr. Mass Spectrom. Relat. Tech.*, Champaign, IL, AOCS Press, 2005, pp. 298–412.
- [54] W.C. Byrdwell, E.A. Emken, Analysis of triglycerides using atmospheric pressure chemical ionization mass spectrometry, *Lipids* 30 (1995) 173–175, doi:10.1007/BF02538272.
- [55] W.C. Byrdwell, The Updated Bottom Up Solution Applied to Atmospheric Pressure Photoionization and Electrospray Ionization Mass Spectrometry, *JAACS, J. Am. Oil Chem. Soc.* 92 (2015) 1533–1547, doi:10.1007/s11746-015-2735-z.
- [56] W.C. Byrdwell, The bottom-up solution to the triacylglycerol lipidome using atmospheric pressure chemical ionization mass spectrometry, *Lipids* 40 (2005) 383–417, doi:10.1007/s11745-006-1398-9.
- [57] W.C. Byrdwell, Breaking the rules: two- and three-dimensional liquid chromatography with four dimensions of mass spectrometry, *Curr. Trends Mass Spectrom.* 19 (2021) 6–11 [https://www.byrdwell.com/Classic/Byrdwell\\_CurrTrendsMassSpectrom\\_19\\_6\\_2021.pdf](https://www.byrdwell.com/Classic/Byrdwell_CurrTrendsMassSpectrom_19_6_2021.pdf).
- [58] H.R. Mottram, R.P. Evershed, Structure analysis of triacylglycerol positional isomers using atmospheric pressure chemical ionisation mass spectrometry, *Tetrahedron Lett.* 37 (1996) 8593–8596, doi:10.1016/0040-4039(96)01964-8.
- [59] M. Holčápek, H. Dvorakova, M. Lísá, A.J. Giron, P. Sandra, J. Cvacka, Regioisomeric analysis of triacylglycerols using silver-ion liquid chromatography-atmospheric pressure chemical ionization mass spectrometry: comparison of five different mass analyzers, *J. Chromatogr. A.* 1217 (2010) 8186–8194, doi:10.1016/j.chroma.2010.10.064.
- [60] T. Řezanka, K. Sigler, Separation of enantiomeric triacylglycerols by chiral-phase HPLC, *Lipids* 49 (2014) 1251–1260, doi:10.1007/s11745-014-3959-7.
- [61] T. Řezanka, K. Pádřová, K. Sigler, Regioisomeric and enantiomeric analysis of triacylglycerols, *Anal. Biochem.* 524 (2017) 3–12, doi:10.1016/j.ab.2016.05.028.
- [62] A. Jakab, I. Jablonkai, E. Forgács, Quantification of the ratio of positional isomer dilinoleoyl-oleoyl glycerols in vegetable oils, *Rapid Commun. Mass Spectrom.* 17 (2003) 2295–2302 <http://www.scopus.com/inward/record.uri?eid=2-s2.0-0141989735&partnerID=40&md5=9e4ca4cdc499795da0fec35f406ae3a9>, doi:10.1002/rcm.1193.
- [63] W.C. Byrdwell, The Updated Bottom Up Solution applied to mass spectrometry of soybean oil in a dietary supplement gelcap, *Anal. Bioanal. Chem.* 407 (2015) 5143–5160, doi:10.1007/s00216-015-8590-9.